Geomatica 76 (2024) 100018

Contents lists available at ScienceDirect

Geomatica

journal homepage: www.sciencedirect.com/journal/geomatica

Mapping winter wheat crop traits dynamic change and growth performance for variable rate application using Sentinel-1 and Sentinel-2

Bing-Bing Goh [a,*], Sheida Z. Sattari [c], Chris J. Bleakley [b], Nicholas M. Holden [a]

[a] School of Biosystems and Food Engineering, University College Dublin, Belfield, Dublin 4, Ireland
[b] School of Computer Science, University College Dublin, Belfield, Dublin 4, Ireland
[c] Origin Enterprises Digital Ltd, HQ Building 329F Wing Thompson Avenue, Harwell Campus, Didcot OX11 0GD United Kingdom

ARTICLE INFO

Keywords:
Precision agriculture
Machine learning
Crop management system
Remote sensing
Fusion

ABSTRACT

Site specific crop management for variable rate application is extensively recognized as a method for distributing agricultural input unevenly across a field, tailored to the diverse requirement of different areas. From the previous study, this approach proven to reduce agricultural input expenses by 10 % without impacting yield and ensure environmental sustainability. This study presents a new approach to delineate management zones for precision agriculture using crop biophysical property variability assessment within winter wheat fields. A multivariate random forest framework was developed to estimate winter wheat's biophysical properties within fields from surface reflectance and backscatters of Sentinel-1 and Sentinel-2. Combining Sentinel-1 and Sentinel-2 data resulted in more precise estimation of the green area index (R^2=0.98), aboveground dry biomass (R^2=0.90), plant height (R^2=0.94), and leaf nitrogen content (R^2=0.78). Sentinel-2 alone was particularly effective in estimating shoot density (R^2=0.94). These estimates were then used to create management zones for precision agriculture, classified based on agronomic performance benchmarks. The fuzzy c-mean clustering algorithm helped generate homogeneous management zones, considering the biophysical variations within fields. The ultimate goal is to integrate these biophysical property maps and management zones into crop management workflows. This integration will assist farmers in recognizing field variability and understanding its causes. Moreover, the spatial distribution of these zones supports variable rate application, guiding farmers towards more efficient, profitable, and sustainable crop management practices.

1. Introduction

Precision agriculture requires the acquisition, processing and analysis of spatial, and temporal data within the fields in order to support management decisions that improve resource usage efficiency, productivity, profitability, and sustainability of agricultural production [51]. With the rising prices of chemicals and fossil fuels, and a growing environmental awareness, farm practices and government policies will precision approaches in order to maximize return while preserving inputs and resources without harming the environment [19]. For precision agriculture, the field is divided into management zones, allowing instantaneous and specific action in each zone within a large field once the management decisions have been made.

As the technology for remote sensing has evolved to offer greater spatial, spectral, radiometric, and temporal resolution, it is integral to precision agriculture with its strength to determine the relationship between surface reflectance or backscatter and soil properties, as well as surface roughness and crop characteristics. It revolutionized the crop growth monitoring with high resolution satellite images from optical and radar sensors. In conjunction with global navigation satellite systems (GNSS), and geographic information systems (GIS), spatial data and information have been used in variable rate application (VRA) for seeding [26], fertilizers [3], crop protection [42], irrigation [30], and growth regulators [17].

The VRA involves applying agricultural inputs at different rates throughout the field according to the management zone. Using VRA, areas that generate the largest return can be targeted for inputs, while reduced inputs to areas with low productivity or where previous management has indicated in lower input requirement [2] can reduce pollution and waste. Additionally, VRA strives to optimize profit margins, as well as ensure environmental sustainability. Although VRA has proven to be successful, interpretation of remote sensing data remains a

* Corresponding author.
E-mail address: eringohbb@gmail.com (B.-B. Goh).

https://doi.org/10.1016/j.geomat.2024.100018
Received 2 June 2024; Received in revised form 5 August 2024; Accepted 10 August 2024
Available online 15 August 2024

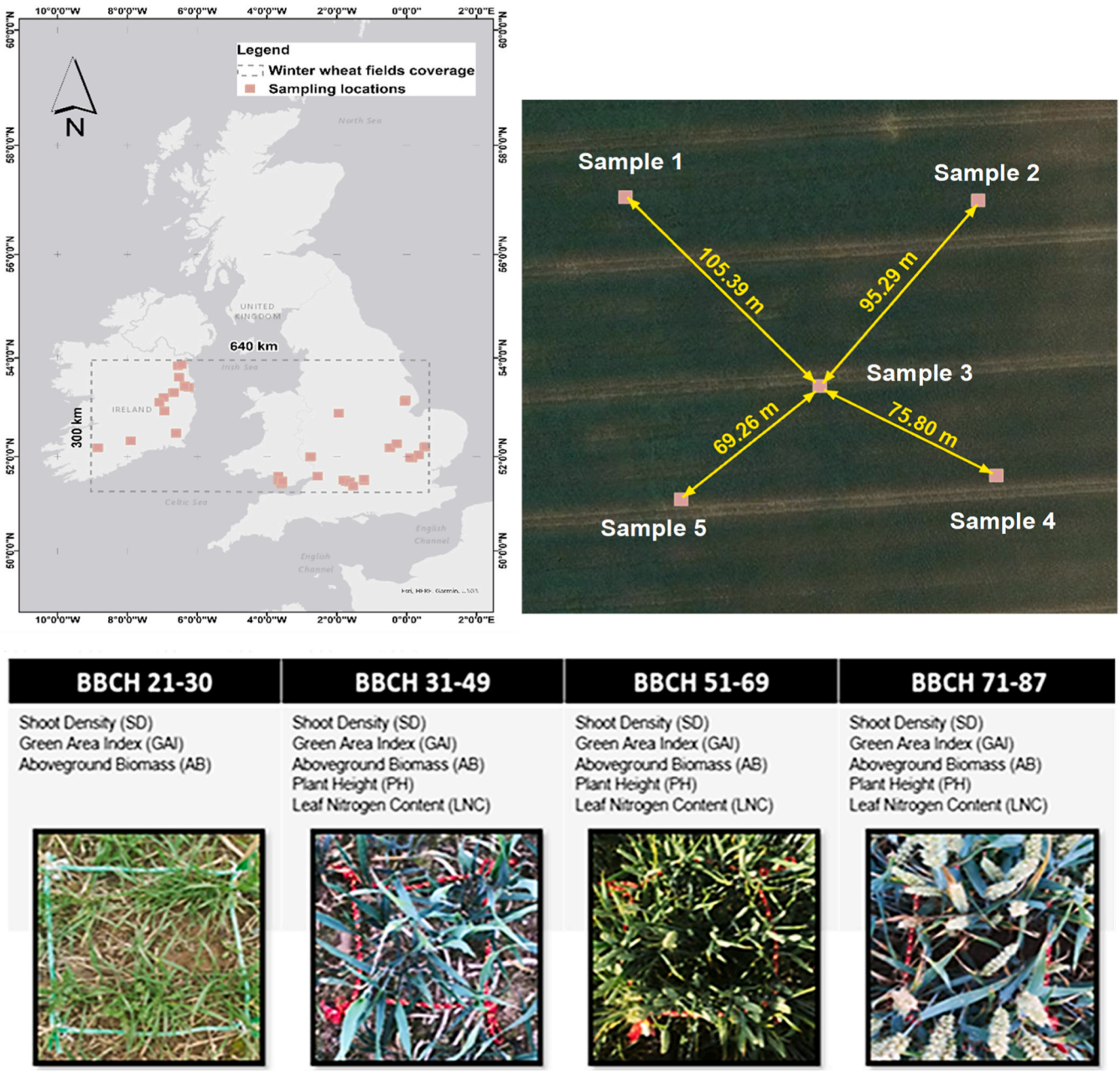

Fig. 1. Ground truth sampling at winter wheat field in Ireland and United Kingdom. The 5 plots sampling design was conducted at each individual winter wheat field for 4 key growth stages over the growing seasons.

challenge for the end users since there is a need for a certain level of expertise and computing [47].

Each field management zone typically has somewhat homogeneous conditions that respond to inputs in a similar manner. By dividing a field into management zones, a farmer can treat each area at the right time, with the right rate, based on crop needs [27]. Even though traditional farming successfully employed uniform management or treatment for the entire field, it is becoming inappropriate to treat high yielding areas in the same manner as low yielding areas. The consequent overuse of chemicals for crop nutrition and plant protection has resulted in contamination of the environment [7]. A study by Ehlert et al., [12] found that 10–12 % of fertilizer can be reduced without affecting wheat yields when site-specific treatments are implemented for each management zone. In the literature, the most commonly used data sources for management zone delineation are soil parameters [6,60], electrical conductivity [9,25], yield maps from harvester [8,15] and vegetation indices (i.e. normalized different vegetation index (NDVI), red edge inflection point (REIP) and soil-adjusted vegetation index (OSAVI)) [49, 56]. However, no detail guideline has been established on which available data attributes contributed to the physical and biological keystone of management zone creation [23]. There is limited research exists on defining crop management zones based on crop biophysical properties (CBP) and agronomic performance benchmark.

Intensive research for CBP retrieval has been explored using optical sensor [16] and radar sensor [48]. CBP retrieval using remote sensing helps to understand winter wheat growth performance through assessing the dynamic changes in shoot density (SD), green area index (GAI), plant height (PH), aboveground dry biomass (AGDB) and leaf nitrogen content (LNC). These provide fundamental information for crop yield formation [41], plant response to pests and diseases [44], environmental change [34], and fertilizer applications [11]. Besides, the key wheat management decisions are associated with the wheat growth stages. The

Table 1
Crop biophysical parameters measurement and method.

In Situ Data	Method
Quadrat location	Latitude and Longitude to the nearest 0.00001 degrees
Growth Stage (GS)	Plant morphology of each quadrat was matched with the BBCH scale description and the specific BBCH code was recorded. Growth stage based on BBCH scale
Shoots Density (SD)	Total count of shoots per quadrat.
Green Area Index (GAI)	The ratio of green leaf and stem area to the area of ground, an average of three measurements from BASF GAI smartphone application per quadrat.
Plant Height (PH)	Average of three above-ground plant height measurements per quadrat using self-retracting metal tape.
Leaf N Concentration (LC%)	Average of ten readings measured by SPAD−502Plus chlorophyll meter from uppermost leaves per quadrat. Calculate the final value using Eq.1From [28] LC% = 0.079(SPAD value) −0.154 Eq. 1
Aboveground Fresh Biomass (AGFB)	Destructive sampling of fresh plants per quadrat. The fresh plants were weighed using a digital weighing scale with a maximum capacity of 5000 g to obtain AGFB. The fresh plant was further split into leaves, stems, and spikes.
Aboveground Dry Biomass (AGDB)	The total weight of oven-dried leaves, stems, and spikes (dried in the oven at 70 °C for 48 h until constant weight) were obtained respectively and also added up to calculate the total aboveground dry biomass.
Leaf Dry Biomass (LDB)	Weight of oven-dried plant leaves per quadrat.
Plant Water Content (PWC)	Subtraction of Aboveground Fresh Biomass and Aboveground Dry Biomass.
Leaf Nitrogen Content (LNC)	Value of Leaf N Concentration multiplies with the Leaf Dry Biomass using Eq.2 to get Leaf N Content from [29]. LNC=LDB x LC% Eq. 2

farmers and agronomists always identify the wheat growth stages by the occurrence of key developmental events of the CBP [20].

With the evidence of successful case studies of using Sentinel-1 and Sentinel-2 in CBP retrieval, we aim to produce crop management zones using predicted CBP from remote sensing data that address the yield limited factors associated with crop trait dynamic change as they become detectable. The research, (1) implements pixel-level fusion method with simple band combinations of sentinel-1 and sentinel-2 to predict 5 CBP (2) generates management zone map based on CBP using the agronomic performance benchmark (3) uses the digital management zone map for variable rate application for seasonal crop management and yield potential forecasting. (4) apply and validate this approach to 4 production fields in the Republic of Ireland and the United Kingdom.

2. Method and materials

2.1. Study area and ground truth sampling

The study area covers the Republic of Ireland and the United Kingdom, involving 75 winter wheat fields for ground truth data collection campaigns over two winter wheat growing cycles. In each field, the ground truth sampling using the 5 plots sampling design at each winter wheat field. Each plot was randomly located at least 20 m away from each other and 10 m from the field boundary to mitigate the edge effect (Fig. 1). Destructive sampling for above ground fresh biomass was conducted using 0.5 m x 0.5 m quadrats at tillering (BBCH21–30), stem elongation (BBCH31–49), heading and flowering (BBCH51–69) and ripening (BBCH71–87) (Fig. 1). In total, 1500 samples were collected across 75 fields, 5 plots and 4 key growth stages.

2.2. Crop biophysical measurements

The crop biophysical measurements of SD, GAI, PH, AGDB, and LNC were summarized in (Table 1).

2.3. Sentinel-1 and Sentinel-2 data

The study used Sentinel-1 and Sentinel-2 images downloaded from Google Earth Engine, timed with field sampling dates. Sentinel-1 image of ± 2 days and Sentinel-2 image of ± 4 days of the sampling date were used. For a detailed timeline of sampling dates and available dates for Sentinel-1 and Sentinel-2 images, see Table S1a and S1b in the supplementary data or supporting information. Pixel values of Sentinel-1 backscatters in (VV and VH) polarization with 10 m resolution and 10 spectral bands of Sentinel-2 (Band 2,3,4,5,6,7,8,8 A,11,12) with (10 m, 10 m, 10 m, 20 m, 20 m, 20 m, 10 m, 20 m, 20 m, 20 m) resolution respectively were extracted based on quadrat's location in latitude and longitude. In the event of unavailability of Sentinel-2 image due to cloud cover, the record affected will be excluded from analysis. The final records paired with Sentinel-1 and Sentinel-2 data are n = 1148 out of 1500 samplings. We applied a data reduction technique, using the locally weighted scatterplot smoothing (LOWESS) algorithm throughout various phenology stages over a wide geographical extent.

2.4. Algorithm to generate site specific CBP maps

This study examined three machine learning algorithms, support vector machine (SVM), random forest regression (RFR) and k-nearest neighbors regression (KNNR). However, based on our final result, RFR outperformed SVR and KNNR. Multivariate random forest regression (RFR) has been proven to be a useful exploratory and predictive tool for

Table 2
Datasets used in this study for modelling each CBP based on different growth stage windows.

Datasets	Input Data	RFR	Scenarios	Growth stages
1	Shoot density, 2 backscatters, 10 spectral	Shoot density	1st	BBCH21 −87
2	Shoot density, 2 backscatters, 10 spectral	Shoot density	2nd	BBCH21 −30
3	Shoot density, 2 backscatters, 10 spectral	Shoot density	3rd	BBCH21 −30BBCH31 −39BBCH40 −71BBCH72 −87
4	Green area index, 2 backscatters, 10 spectral	Green area index	1st	BBCH21 −87
5	Green area index, 2 backscatters, 10 spectral	Green area index	2nd	BBCH21 −59
6	Green area index, 2 backscatters, 10 spectral	Green area index	3rd	BBCH21 −30BBCH31 −39BBCH40 −71BBCH72 −87
7	Plant height, 2 backscatters, 10 spectral	Plant height	1st	BBCH31 −87
8	Plant height, 2 backscatters, 10 spectral	Plant height	2nd	BBCH31 −71
9	Plant height, 2 backscatters, 10 spectral	Plant height	3rd	BBCH31 −39BBCH40 −71BBCH72 −87
10	Aboveground dry biomass, 2 backscatters, 10 spectral	Aboveground dry biomass	1st & 2nd	BBCH21 −87
11	Aboveground dry biomass, 2 backscatters, 10 spectral	Aboveground dry biomass	3rd	BBCH21 −30BBCH31 −39BBCH40 −71BBCH72 −87
12	Leaf nitrogen content, 2 backscatters, 10 spectral	Leaf nitrogen content	1st	BBCH30 −87
13	Leaf nitrogen content, 2 backscatters, 10 spectral	Leaf nitrogen content	2nd	BBCH30 −39
14	Leaf nitrogen content, 2 backscatters, 10 spectral	Leaf nitrogen content	3rd	BBCH30 −39BBCH40 −71BBCH72 −87

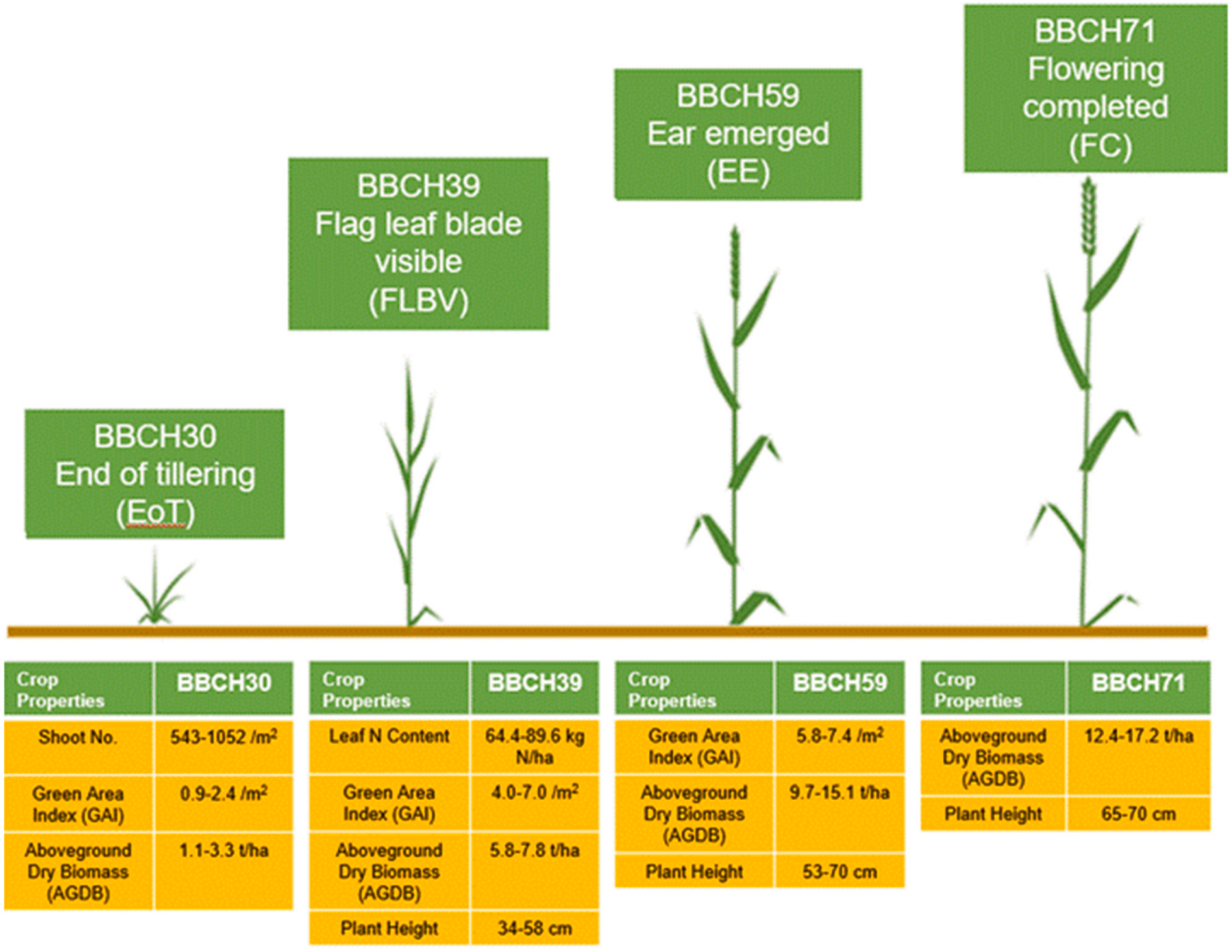

Fig. 2. Benchmark values for CBP at key growth stages for winter wheat growth monitoring derived from Teagasc [31] and AHDB [52].

Table 3
Summaries of 4 production fields for testing purpose.

Country	Wheat Field	Location (Degrees) Latitude, Longitude	Growth Season	Sowing Date	Yield (t/ha)	Area (ha)
Ireland	Ward 2	−6.360119, 53.441602	2019/20	26/10/2019	3.8	75.8
Ireland	Meath1	−6.591134, 53.631634	2020/21	14/09/2020	12.2	8.4
United Kingdom	Hazel8	−2.557953, 51.590988	2019/20	29/10/2019	4.9	7.8
United Kingdom	FlaxClose	−2.766059, 51.991647	2020/21	15/09/2020	11.6	14.1

estimating CBP [35,59], and handling multicollinearity problems [10,18]. The 2 backscatter parameters and 10 spectral bands as predictors in the models. SD, GAI, PH, AGDB and LNC as response variables and total n = 1148 input data were further sorted by each CBP and growth stage to construct 3 different dataset scenarios for modelling. (Table 2) shows three scenarios modeled crop traits across growth stages, with the first scenario spanning from tillering to ripening (BBCH21–87), the second scenario focusing on changes of each CBP in increasing trend. For example, by nature, a healthy winter wheat has an increasing GAI trend from tillering (BBCH21) and normally ends when ear emerged (BBCH59). Thereafter, the trend of GAI ceases due to senescence, it is meaningless to monitor GAI after BBCH59 with no insightful message to the crop growth condition. The third scenario on narrower window of 4 key growth stages. AGDB has increasing trend from BBCH21–87, thus, there's no different between 1st and 2nd scenarios of its modelling. The third scenario is modelling the CBP with narrower window which is 4 key growth stages. However, PH and LNC were modeled in 3 key growth stages because both were not measurable yet during tillering.

The data was split into ¾ training and ¼ testing datasets. 10-fold cross validation was applied to optimize these two algorithms. Model performance was gauged by coefficient of determination (R^2), root mean square errors (RMSE) and normalized root mean square error (NRMSE %) with higher R^2 indicating better prediction accuracy.

2.5. Delineation of management zones in wheat fields using CBP maps

CBP maps generated in Section 3.5 make informed decisions by classifying zones based on crop growth and yield. There was lack of study on delineation of crop management zone using the CBP. This study introduces a method using these properties to delineate management zones in winter wheat and comparing them to benchmarks values (Fig. 2) indicated crop has achieved optimum yield at 10 t/ha. Fuzzy c-means unsupervised clustering algorithm was used to classify the crop management zone classes to "below target", "on target" and "exceed

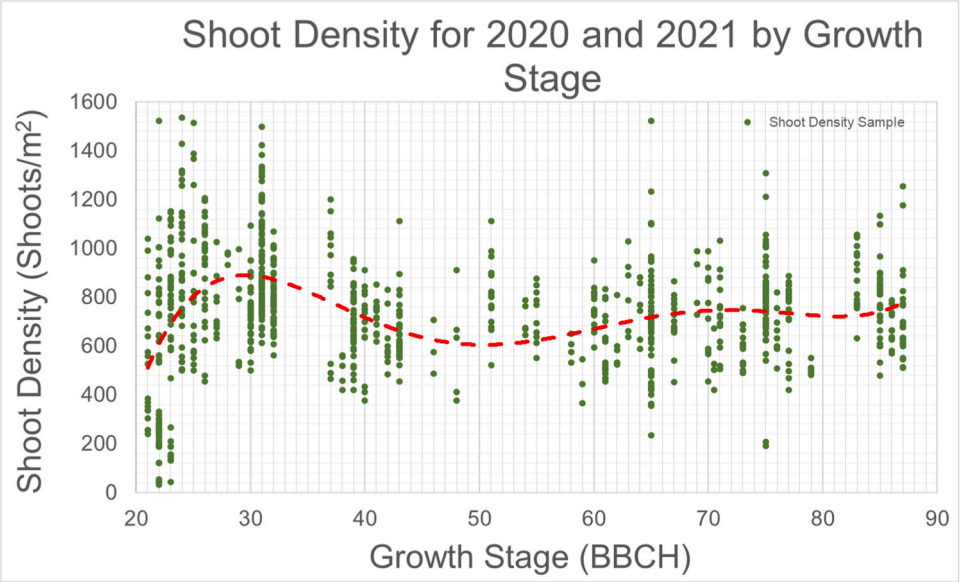

Fig. 3. The trend of observed winter wheat SD at different growth stages.

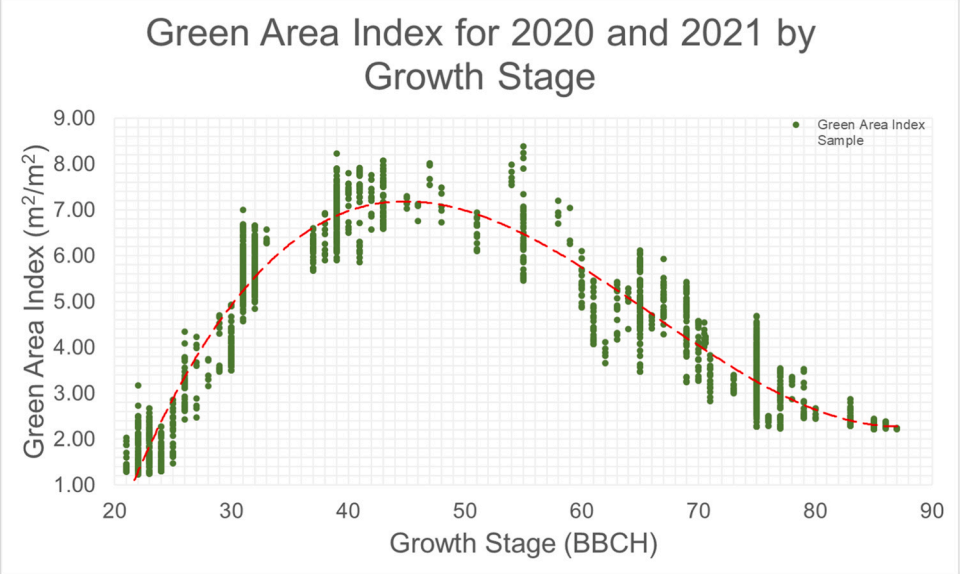

Fig. 4. The trend of observed winter wheat GAI at different growth stages.

target" to discriminate the crop growth performance. This algorithm handles the data uncertainty by allowing data points to belong to multiple clusters simultaneously associate with probability score for each cluster. The crop management zone classes offered potential to adjust input application (fertilizer, herbicide, pesticide, fungicide and plant growth regulator) that matched the crop needs. 4 production fields (Table 3) were mapped, representing high and low yields from IE and the UK.

3. Results

3.1. Crop traits dynamic change based on 5 CBP collected over 2 crop growth cycles

In-situ crop traits were monitored to observe morphological changes throughout the growth stages. There was no change to the AGDB dataset because its morphology development started at beginning of tillering stage (BBCH21) and continued throughout the full growth stages (Fig. 5). SD decreased after end of tillering (BBCH30) (Fig. 3), GAI peaked then stopped at ear emerged (BBCH59) and declined thereafter (discussed below, presented in (Fig. 4), PH developed while the stem was growing until the beginning of flowering stage (BBCH61) and stagnated thereafter (Fig. 6). The change of LNC rose during stem elongation (BBCH30–39) and canopy expansion (Fig. 7). Each CBP are crucial for developing the estimation models.

3.1.1. In-situ (SD)

The emergence of the side shoots at the leaf stem junction of winter wheat plant starts at BBCH21 and peaking at BBCH30 (Fig. 3). The SD ranges from 613 shoots/m^2 to a maximum of 1500 shoots/m^2 after BBCH30.

3.1.2. In-situ (GAI)

It is apparent from the observed GAI in (Fig. 4), the canopy

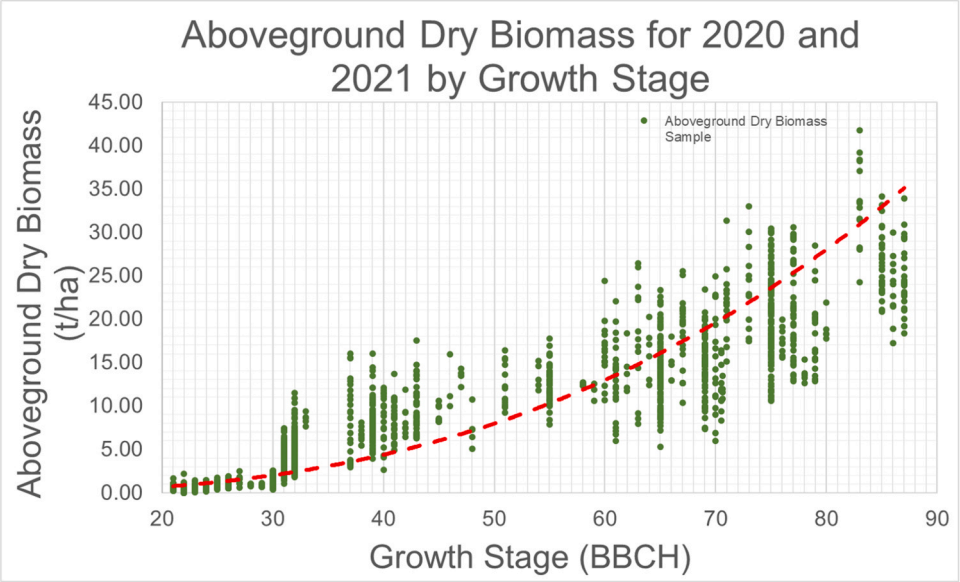

Fig. 5. The trend of observed winter wheat AGDB at different growth stages.

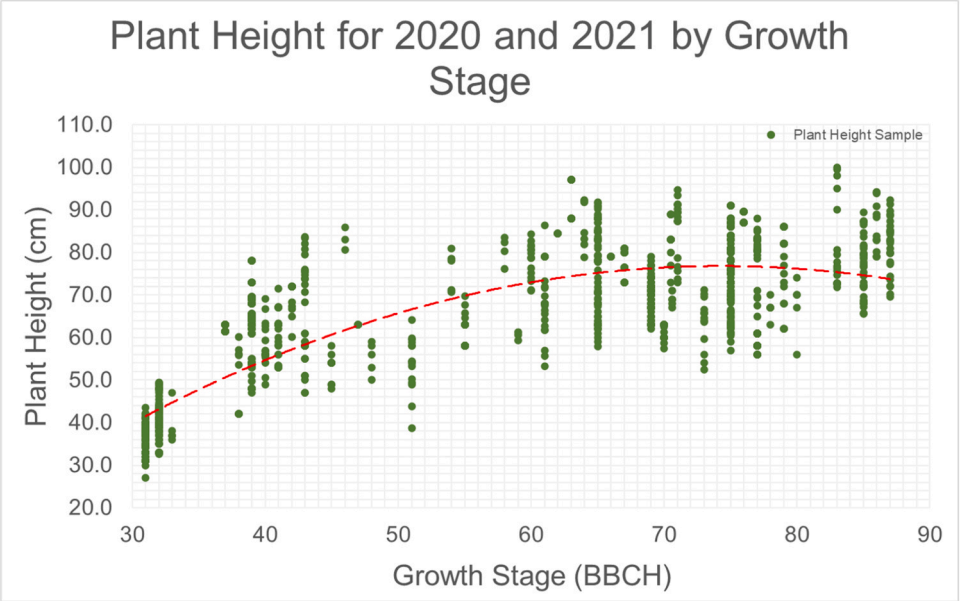

Fig. 6. The trend of observed winter wheat PH at different growth stages.

expansion of winter wheat begins at tillering (BBCH21) and ends after the ear emerged (BBCH59). The GAI reaches a maximum of 8.00 m^2/m^2 to 8.4 m^2/m^2 at flag leaf visible (BBCH39) to ear emerging (BBCH56) (Fig. 4). Declines in GAI during this period may signal disease [5] or drought [37]. Once the end of heading, the GAI starts to decrease as a result of leaves senescence.

3.1.3. In-situ (AGDB)

(Fig. 5) indicates how the observed wheat AGDB has changed over the growing season. AGDB growth is minimal before BBCH30 due to cold weather. It surges at stem elongation (BBCH31), until the ear emergence (BBCH59). From BBCH59 to BBCH71, AGDB increases rapidly as stem and ear biomass accumulate. At the end of flowering stage (BBCH71), the stem biomass ceases and only grain accumulates AGDB, peaking at early dough (BBCH83), then declines due canopy senescence, leaf loss, and ongoing plant respiration [20,52].

3.1.4. In-situ (PH)

(Fig. 6) shows that the PH rapidly increases to 64 cm at flag leaf visible (BBCH39) and then at a gradual rate until its final height between beginning of flowering (BBCH61) to end of flowering (BBCH71) in (Fig. 6).

3.1.5. In-situ (LNC)

(Fig. 7) illustrates the differences in observed LNC at different growth stages in the study area. Observed leaf nitrogen uptake begins at stem elongation BBCH30, and peak at BBCH37, when flag leaf emerges. LNC declines after heading (BBCH51) as nutrient transfer to develop grains [57].

3.2. Models' performance of fusing radar (Sentinel-1) and optical (Sentinel-2) sensors using RFR

(Table 4) shows RFR model of fused Sentinel-1 and Sentinel-2 to

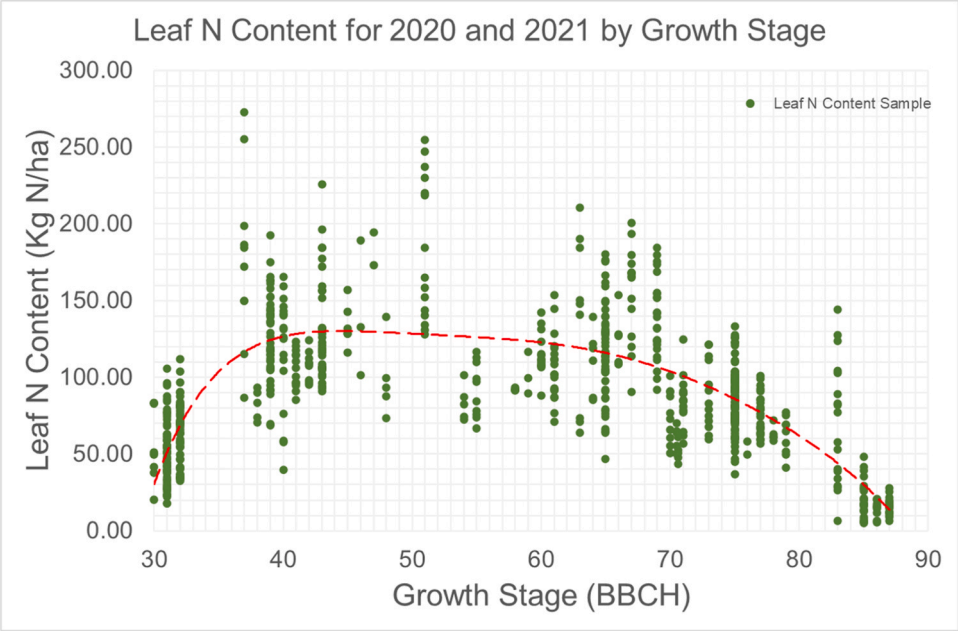

Fig. 7. The trend of observed winter wheat LNC at different growth stages.

Table 4
Performance of combined Sentinel-1 and Sentinel-2 to estimate CBP throughout full growth stages using random forest regression.

Crop biophysical properties	Growth stages	Training Dataset			Testing Dataset		
		R^2	RMSE	NRMSE	R^2	RMSE	NRMSE
SD ($Shoots/m^2$)	BBCH21 −87	0.49	151	0.13	0.65	102	0.10
GAI (m^2/m^2)	BBCH21 −87	0.96	0.39	0.05	0.97	0.32	0.05
AGDB (t/ha)	BBCH21 −87	0.90	2.49	0.06	0.90	2.47	0.07
PH (cm)	BBCH21 −87	0.93	5.02	0.05	0.94	4.62	0.05
LNC (Kg N/ha)	BBCH21 −87	0.74	26.28	0.08	0.73	29.11	0.08

Table 5
Performance of combined Sentinel-1 and Sentinel-2 to estimate CBP at specific growth stages window using random forest regression.

Crop biophysical properties	Growth stages	Training Dataset			Testing Dataset		
		R^2	RMSE	NRMSE	R^2	RMSE	NRMSE
SD ($Shoots/m^2$)	BBCH21 −30	0.69	155	0.13	0.87	75	0.08
GAI (m^2/m^2)	BBCH21 −59	0.97	0.37	0.05	***0.98***	0.34	0.05
AGDB (t/ha)	BBCH21 −87	0.90	2.49	0.06	***0.90***	2.47	0.07
PH (cm)	BBCH31 −87	0.94	4.28	0.05	***0.94***	4.45	0.06
LNC (Kg N/ha)	BBCH30 −39	0.79	26.41	0.08	***0.78***	29.04	0.09

estimate SD, GAI, AGDB, PH and LNC. RFR models consistently showed high predictive ability for all 5 CBP with R^2 between 0.65 – 0.97 using testing dataset. The GAI, AGDB and PH, RFR models indicated a good fit of the fusion method to estimate these 3 crop properties of winter wheat field from tillering until ripening.

The results of 2nd modelling scenario are listed in (Table 5). This scenario only investigated the backscatters and spectral bands of the CBP during a specific growth stage window when the CBP develops and in a growing trend.

The 3rd scenario in (Table 6) which splits the dataset further into 4 key growth stages with narrower time window. The prediction performances varying across different key growth stages for different CBP from R^2 between (0.22–0.95). The SD model has the best prediction performance at tillering stage $R^2 = 0.87$, GAI at heading and flowering stage $R^2 = 0.93$, AGDB and PH at stem elongation stage $R^2 = 0.72$ and $R^2 = 0.95$ respectively, and LNC at both stem elongation $R^2 = 0.78$ and fruiting stages $R^2 = 0.78$.

3.3. Models' performance of single optical sensor (Sentinel-2) using RFR

In this study, the comparison between the fusion sensors' model and single sensor's model were investigated. The best performance fusion model has been developed using 2nd scenario. Thus, to investigate the performance of using single optical sensor and single radar sensor, the 2nd scenario was adopted in modelling. The result of using Sentinel-2 sensor only is in (Table 7). The single optical sensor (Sentinel-2)

Table 6
Performance of combined Sentinel-1 and Sentinel-2 to estimate CBP at four/three key growth stages using random forest regression.

Crop biophysical properties	Growth stages	Training Dataset			Testing Dataset		
		R^2	RMSE	NRMSE	R^2	RMSE	NRMSE
SD (Shoots/m^2)	BBCH21 −30	0.69	155	0.13	0.87	75	0.08
	BBCH31 −39	0.39	147	0.16	0.55	114	0.17
	BBCH40- 71	0.25	147	0.15	0.22	119	0.21
	BBCH72 −87	0.47	144	0.14	0.65	81	0.14
GAI (m^2/m^2)	BBCH21 −30	0.59	0.31	0.10	0.71	0.25	0.14
	BBCH31 −39	0.77	0.37	0.09	0.78	0.37	0.09
	BBCH40- 71	0.89	0.47	0.09	0.93	0.36	0.07
	BBCH72 −87	0.81	0.27	0.11	0.85	0.25	0.11
AGDB (t/ha)	BBCH21 −30	0.71	0.27	0.11	0.68	0.28	0.12
	BBCH31 −39	0.68	1.77	0.09	0.72	1.62	0.12
	BBCH40- 71	0.61	2.92	0.10	0.67	2.94	0.13
	BBCH72 −87	0.72	3.80	0.11	0.66	4.03	0.17
PH (cm)	BBCH31 −39	0.93	3.58	0.06	0.95	3.27	0.05
	BBCH40- 71	0.81	4.96	0.09	0.79	5.42	0.10
	BBCH72 −87	0.71	7.85	0.08	0.78	6.71	0.07
LNC (Kg N/ha)	BBCH31 −39	0.79	26.41	0.08	0.78	29.04	0.09
	BBCH40- 71	0.52	26.84	0.12	0.48	33.72	0.17
	BBCH72 −87	0.85	15.52	0.11	0.78	17.09	0.18

Table 7
Performance of Sentinel-2 sensor to estimate CBP at specific growth stages window using random forest regression.

Crop biophysical properties	Growth stages	Training Dataset			Testing Dataset		
		R^2	RMSE	NRMSE	R^2	RMSE	NRMSE
SD (Shoots/m^2)	BBCH21 −30	0.63	168	0.14	***0.94***	53	0.05
GAI (m^2/m^2)	BBCH21 −59	0.90	0.72	0.10	0.89	0.72	0.10
AGDB (t/ha)	BBCH21 −87	0.66	4.58	0.11	0.78	3.91	0.12
PH (cm)	BBCH31 −87	0.82	7.52	0.10	0.86	6.62	0.08
LNC (Kg N/ha)	BBCH30 −39	0.73	28.76	0.09	0.78	29.84	0.09

demonstrated a good fit to estimate the CBP with R^2 between 0.78–0.94.

3.4. Best performance CBP RFR models

The scatter plots in (Fig. 8) show the model performance, with (Fig. 8*a*) focusing on Sentinel-2 data for SD prediction. Models using fusion data (Fig. 8*b-f*) predicted SD, GAI, AGDB, PH and LNC effectively, demonstrating good linear fits with R^2 of 0.78 (LNC), R^2 of 0.87 (SD), R^2 of 0.90 (AGDB), R^2 of 0.94 (PH), and R^2 of 0.98 (GAI).

3.5. Variable importance of best performance CBP RFR models

Variable importance (VI) of RFR models for CBP prediction in (Fig. 9) shows ranking of spectral and backscatter variables based on importance values. The higher the importance value of a variable indicates the more effective the nodes were split based on best predictor. (Fig. 9*a and b*) demonstrated shoots density model is best with Sentinel-2 where spectral bands are top 8 best predictors in the model. Near infrared, B8 and visible red, B4 played important roles in SD prediction. Sentinel-1 VH and VV backscatters are top influencers in GAI, AGDB and PH prediction models (Fig. 9*c,d,e*). (Fig. 9f) reveals that VV backscatter and red edge, B5 are most important for LNC prediction.

3.6. Management zone maps of 4 production fields at key growth stages

3.6.1. Tillering stage

The SD maps reveal crop response to the 1st split nitrogen, phosphorus and potassium. 3 production fields (Meath1, Hazel8 and FlaxClose) showed positive responded, exceeding 543 shoots/m^2 while Ward2 underperformed due to seed loss after the rainstorm in early February 2020. (Fig. 10) proves that the low SD areas are bare soil, and this is further validated by the farmer's note. Farmers use these maps to focus on management zones with "on target" and "exceed target" for decisions like crop switching or variable rate seeding for optimal outcomes. In addition, Excessive SD may prompt PGR application.

3.6.2. Stem elongation stage

Hazel8 shows sign of underperformance from leaf nitrogen content maps indicated level critical for nitrogen uptake of leaf and nitrogen use efficiency for crop production. This is critical stage to make sure flag leaves of wheat have sufficient nitrogen to contribute to photosynthetic performance during fruiting [32]. Ward2 and Hazel8 fall below the baseline of leaf nitrogen uptake after 2nd and 3rd nitrogen split applications. Hazel8 were detected to have decreasing GAI and AGDB, showing sign of drought and disease.

3.6.3. Heading and flowering stage

From the maps, both Ward2 and Hazel8 unlikely to achieve the target yield at this stage. No additional input was provided by the farmers for these two fields.

3.6.4. Fruiting stage

The maps show Ward2 and Hazel8 did not achieve the target yield. Contrarily, both Meath1 and FlaxClose have achieved the target yield. For milling wheat, farmers continue referring to the maps to identify "on target" and "above target" zone for variable rate application to increase grain protein content.

3.7. Integrating CBP maps in crop management

Diagram in (Fig. 15) summarize the winter wheat crop management throughout the growing season. The diagram integrates the CBP maps

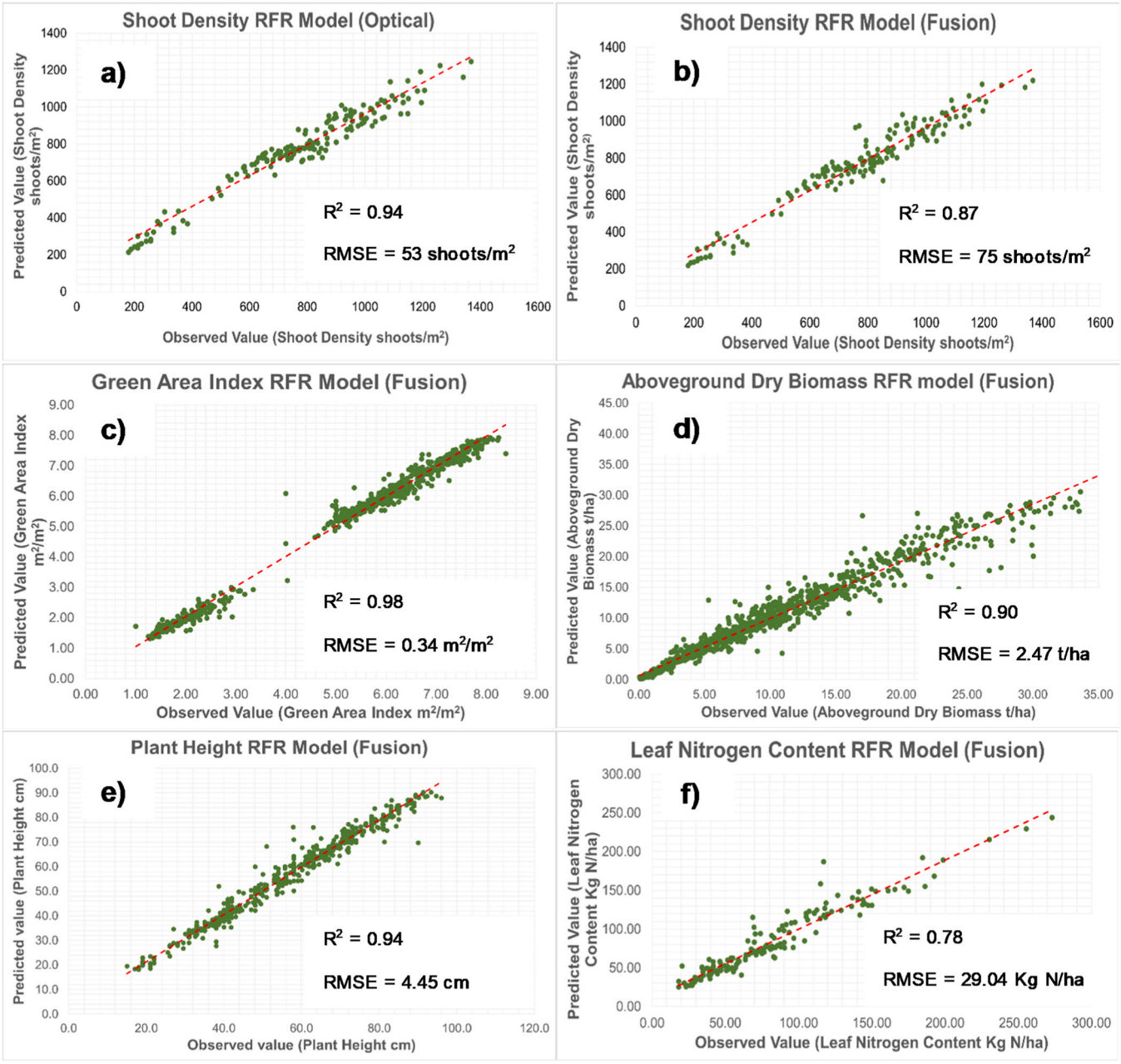

Fig. 8. Scatter plots of observed and predicted CBP of RFR models. One point represents a crop sampling plot (a) SD prediction using Sentinel-2 (b) SD prediction using fusion (c) GAI prediction using fusion (d) AGDB prediction using fusion (e) PH prediction using fusion (f) LNC prediction using fusion.

generate as part of the workflow to assist grower in decision making before and after each crop management steps.

3.8. Integrating CBP maps in yield forecasting

(Table 8) outlines a method to evaluate crop performance CBP map. It calculates the coverage percentages of different management zones and the mean values of these properties at crucial growth stages. Additionally, it assesses whether the field is on track to achieve potential yield of 10 t/ha under the current conditions. The formulas used for these calculations are:

$$bt\% = P_{bt} \div \sum P \tag{3}$$

$$ot\% = P_{ot} \div \sum P \tag{4}$$

$$et\% = P_{et} \div \sum P \tag{5}$$

$$\mu CBP = \frac{1}{P} \sum_{i=1}^{P} CBP \tag{6}$$

Where:

- P_{bt}, P_{ot}, P_{et} are number of pixels fall in below target, on target, exceed target zone respectively.
- bt%, ot%, et% are percentage of below target, on target, and exceed target zone coverage respectively.
- $\sum$ P is total number of pixels fall within a field boundary.
- μCBP is mean value of the crop biophysical properties.
- CBP represents the dataset value for each property.

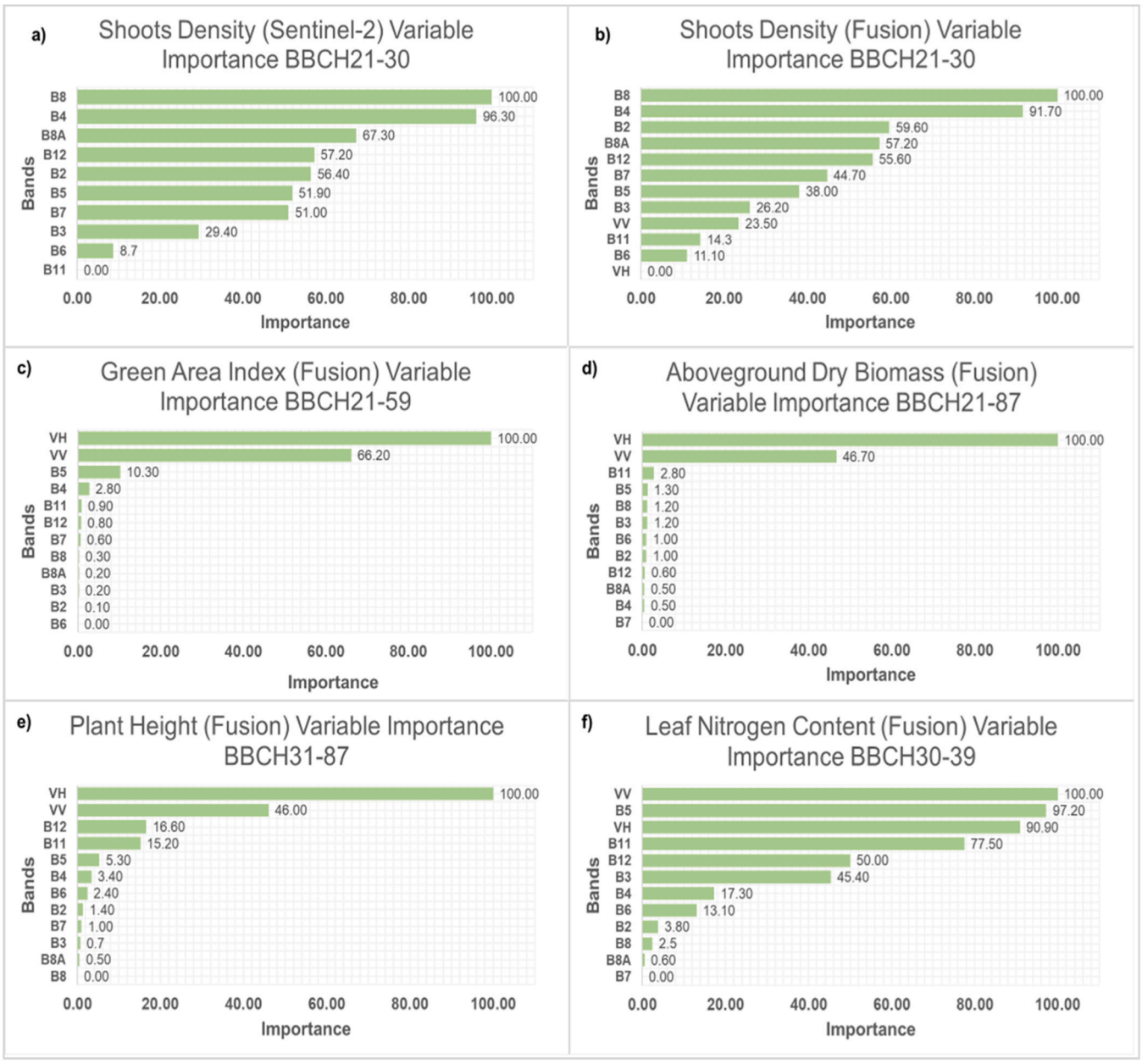

Fig. 9. VI of CBP RFR prediction model of (a) SD using Sentinel-2 only (b) Shoots density using fusion (c) GAI using fusion (d) AGDB using fusion (e) PH using fusion (f) LNC using fusion.

4. Discussions

4.1. Crop traits dynamic change and growth performance benchmark

The trend of each CBP change was observed over 2 growth cycle to identify best specific window for crop modelling and to measure crop growth performance. SD per unit area could help to monitor winter wheat growth and yield [53]. Considering that each shoot has potential to form a spike and vital for yield improvement strategies [4]. After the stem elongation (BBCH31), SD decreases and fluctuates until ripening (BBCH87) (Fig. 3). The UK's optimal final SD for maximum yield is at least 460 shoots/m^2 [52] and while in IE, is 480–600 shoots/m^2 [31] by BBCH31.

Canopy size is crucial for photosynthesis capacity. To determine the radiation interception capacity of a crop, the canopy size is measured using GAI. GAI measured the total surface area of the green components of the canopy including leaves, stems, and ears divided by the ground surface area. Real-time measurement of GAI informs farmers about crop health and guides nitrogen management [46]. Monitoring GAI during BBCH21–59 is essential to find out the effective amount and timing of fertilizer N applied and disease control measures and less important when GAI senesces from June onward which is after BBCH59.

Throughout the whole crop cycle, AGDB prediction is key for crop health assessment, decision-making on optimal crop management strategies, and grain yield forecasts [22]. PH is another predominant CBP influencing wheat yield, morphological change, and lodging resistance [58]. Several studies found a significant negative correlation between wheat grain yield and PH [14,21]. Taller wheat cultivars are more susceptible to lodging risk and a reduction in grain yield. PH is determined by the stem extension which begins at BBCH31.

Farmer also need to understand wheat's nitrogen requirements for effective fertilization [50]. LNC is crucial for photosynthetic activity and grain nutrition [55]. It has significant interaction in response to plant growth regulator accumulate split nitrogen applications at tillering

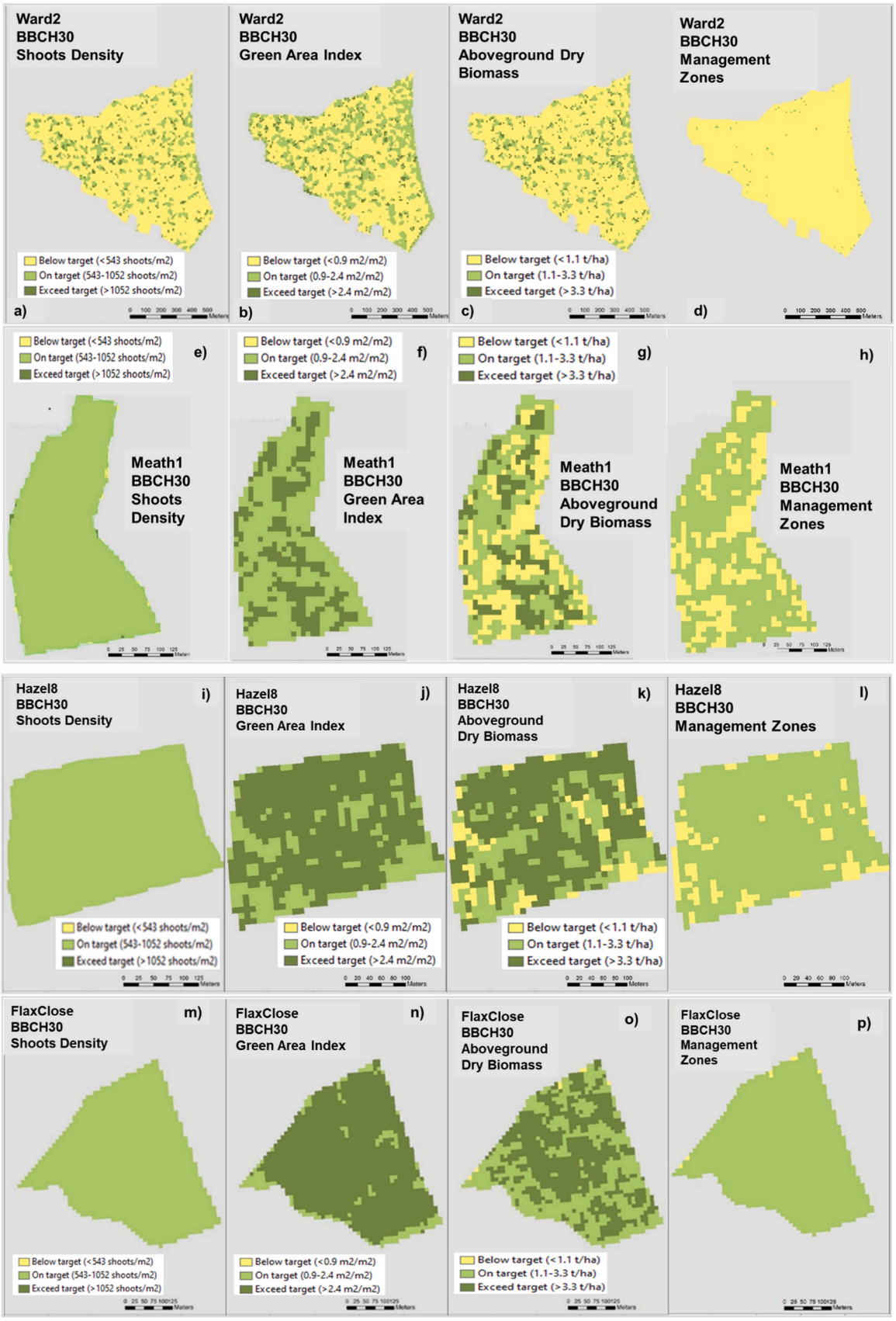

Fig. 10. Delineation of management zones in Ward2, Meath1, Hazel8, and FlaxClose wheat fields during BBCH 30 (end of tillering) using SD, GAI, and AGDB maps.

Table 8
Summary of crop performance of the 4 production wheat fields in percentage, mean crop properties values and achievement of potential target yield (10 t/ha) monitoring at 4 key growth stages.

		Tillering			Stem Elongation				Heading & Flowering			Fruiting	
		SD Shoot/m^2	GAI m^2/m^2	AGDB t/ha	LNC Kg N/ha	GAI m^2/m^2	AGDB t/ha	PH cm	GAI m^2/m^2	AGDB t/ha	PH cm	AGDB t/ha	PH cm
Ward2	Below target (bt%)	79	64	79	65	51	78	63	100	94	96	92	97
	On target (ot%)	21	31	16	33	49	5	32	0	4	4	7	1
	Exceed target (et%)	0	5	5	2	0	17	5	0	2	0	1	2
	Mean μ	185	0.68	0.74	62.56	4.00	2.99	42.7	2.25	2.15	36.3	5.90	45.3
Achieving good yield (10 t/ha)?		**No**			**No**				**No**			**No**	
Meath1	Below target (bt%)	0	0	33	0	20	22	0	15	44	21	28	37
	On target (ot%)	100	67	43	6	69	9	32	75	44	32	43	12
	Exceed target (et%)	0	33	24	94	11	69	68	10	12	47	29	51
	Mean μ	834	2.56	4.10	139.33	5.49	9.72	64.0	6.58	12.52	67.9	14.67	67.4
Achieving good yield (10 t/ha)?		**Yes**			**Yes**				**Yes**			**Yes**	
Hazel8	Below target (bt%)	1	28	12	65.5	46	53	13	97	73	79	85	99
	On target (ot%)	99	72	30	33.5	54	4	58	3	13	21	7	1
	Exceed target (et%)	0	0	58	1	0	43	29	0	14	0	8	0
	Mean μ	791	3.52	7.22	62	4.23	7.59	46.09	3.21	5.96	34.9	4.77	33
Achieving good yield (10 t/ha)?		**Yes**			**Yes, at border line**				**No**			**No**	
FlaxClose	Below target (bt%)	0	0	1	2	8	11	1	14	28	10	44	32
	On target (ot%)	100	11	48.5	12	39	13	16	59	34	30	37	15
	Exceed target (et%)	0	89	50.5	86	53	76	83	27	38	60	19	53
	Mean μ	939	3.8	6.13	105.46	6.45	10.44	65.7	5.66	12.92	69.9	12.23	67.1
Achieving good yield (10 t/ha)?		**Yes**			**Yes**				**Yes**			**Yes**	

(BBCH21–26), stem elongation (BBCH30–32) and flag leaf emerged (BBCH37–39) [40,43].

4.2. Models' performance, uncertainty and variable importance

The models' performance of 2nd scenario *in* (Table 5) has improved the prediction performance of SD, GAI, PH and LNC compared to the results of 1st scenario in (Table 4) *and 3rd scenario in* (Table 6). AGDB remained equal prediction performance because both 1st scenario and 2nd scenario are the same. 2nd scenario overall achieved excellent R^2 between (0.78 – 0.98) for 5 crop properties' testing datasets using fused sensors. However, if single optical sensor (Sentinel-2) was used, the Sentinel-2 sensor yielded better performance in estimating SD (R^2 =0.94) only. The GAI prediction model shows a gap separates predicted GAI data into two clusters (Fig. 8c) is due to no data collected during BBCH32–36 because of COVID19 restriction in 2020 and extreme weather in 2021. Thus, no values for GAI around 4–5 m^2/m^2. (Fig. 8*d*) *shows underfitting for AGDB prediction model when AGDB > 30 t/ha.* The overall variable importance of results showed VH was the most influential Sentinel-1 backscatter parameter to GAI, AGDB and PH. This is likely the volume scattering mechanisms of the crop. The studies of [13,33,39] found VV has demonstrated high correlations with LAI and biomass of wheat. From the findings VV has influence to all the CBP prediction models. This is primarily due to the change of the surface soil as the crop canopy decreased due to the increasing attenuation from the predominantly vertical structure of wheat stems [1]. The results proven that fusing Sentinel-1 and Sentinel-2 improves the CBP predictions. The findings also support and align with previous work in [16] that a single vegetation index (VI) is insufficient and do not have a uniquely predictive relationship with specific biophysical properties. VI can be difficult to untangle and identify exactly which properties are causing a given VI value at a given time and location.

4.3. Integrating CBP maps in crop management and yield forecasting at key growth stages

At tillering stage, farmers refer to the management zones (Fig. 10*a-l*) derived from the predicted crop biophysical maps, classified based on the benchmark values at different key growth stages to (1) gauge crop response post-herbicide spray (BBCH14–21) and 1st split of nitrogen, phosphorus, potassium applications (BBCH25–30) at field. (2) adjust management for fungicide spray (BBCH31–33), plant growth regulator (PGR) application (BBCH30–32 and BBCH37), 2nd split of nitrogen application (BBCH32), and 3rd split of nitrogen application (BBCH37). (3) to find out if the target yield of 10 t/ha is achievable by the wheat field. Variation in SD, GAI and AGDB maps show different management zones, keep farmers informed of chemical and fertilizer needs and utilized the variable rate technology for next applications. The information aids in early yield prediction.

During stem elongation, farmers analyze (Fig. 11a-p) to assess nitrogen efficiency post-2nd and 3rd nitrogen applications, apply variable rate fungicide at BBCH 39 after flag leaf fully emerged and evaluate if target yield of 10 t/ha is achievable. Farmers can consider variable rate application for fungicide which targeted "on target", and "exceed target" management zones with well grow flag leaf crops to reduce costs and losses. (Table 8) predicts the potential of each field in achieving the good yield of 10 t/ha based on management zones.

Throughout heading and flowering stages, (Fig. 12*a-l*) help assess canopy size for nitrogen use efficiency [45], crop health condition for fungicide application, and to find out if the target yield of 10 t/ha is attainable.

When fruiting stage, if milling wheat has been grown, the maps (Fig. 13*a-h*) assist farmers to identify the spatial distribution of high potential yield zone for variable rate application to increase grain protein content.

The CBP maps are also integrated in yield forecasting using the results from (Table 8). It provides valuable insights for calculating input cost and detecting early if the farm can achieve the potential yield as early at the tillering stage. When integrated with management zone maps and crop management workflows, this data is transformed into a Digital Twins representation. This digital model enables farmers to monitor and manage their operations remotely and simulate preventive measures [54].

5. Conclusion

In precision agriculture, management zones play a crucial role in assessing field status and requirements. These zones delineate portions of land within a field that share similar characteristic relevant to crop performance and yield. This study highlights an innovative approach by leveraging CBP derived from satellite remote sensing to produce an appropriate segmentation of management zones.

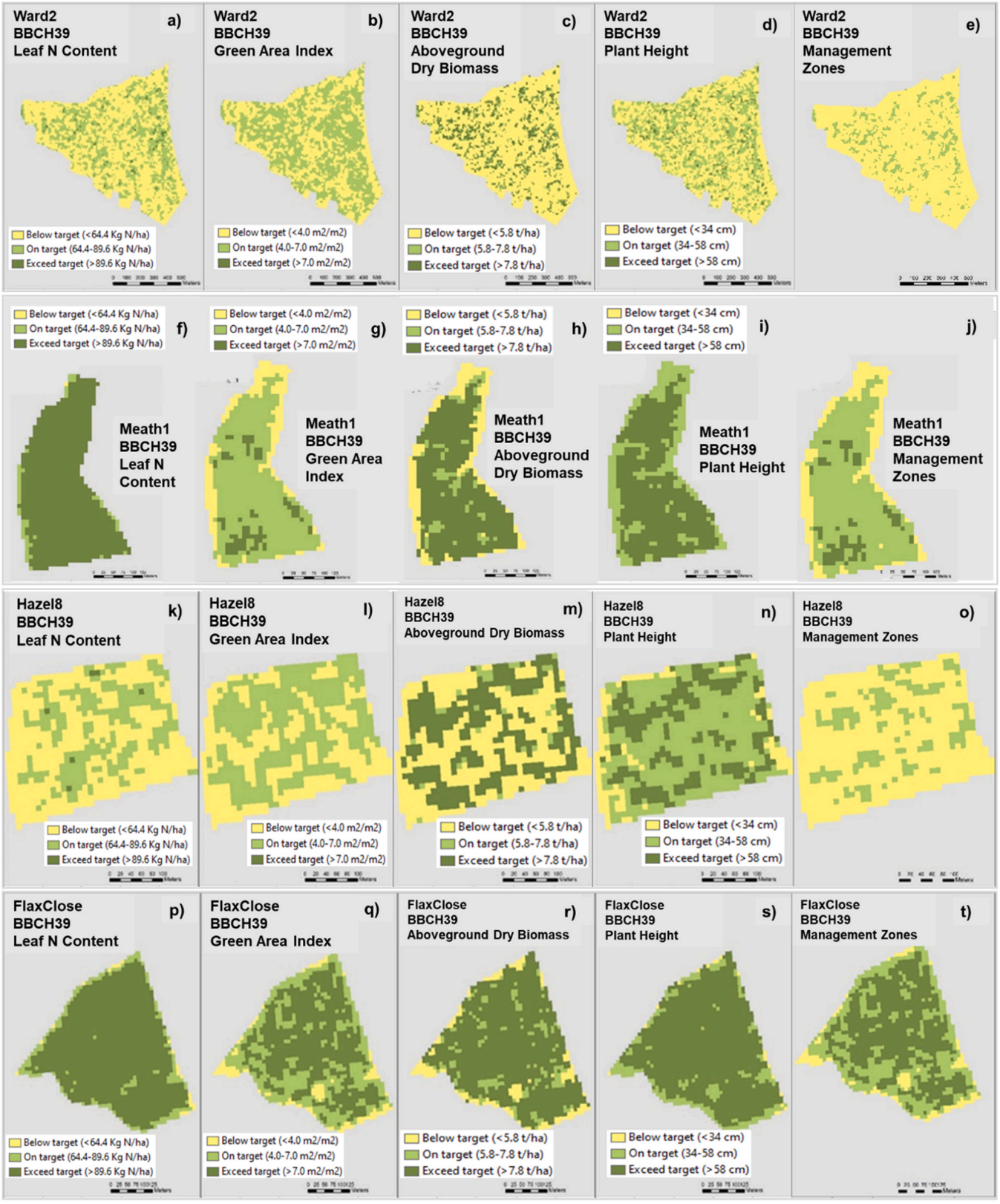

Fig. 11. Delineation of management zones in Ward2, Meath1, Hazel8, and FlaxClose wheat fields during BBCH 39 (Flag leaf blade visible) using LNC, GAI, AGDB and PH maps.

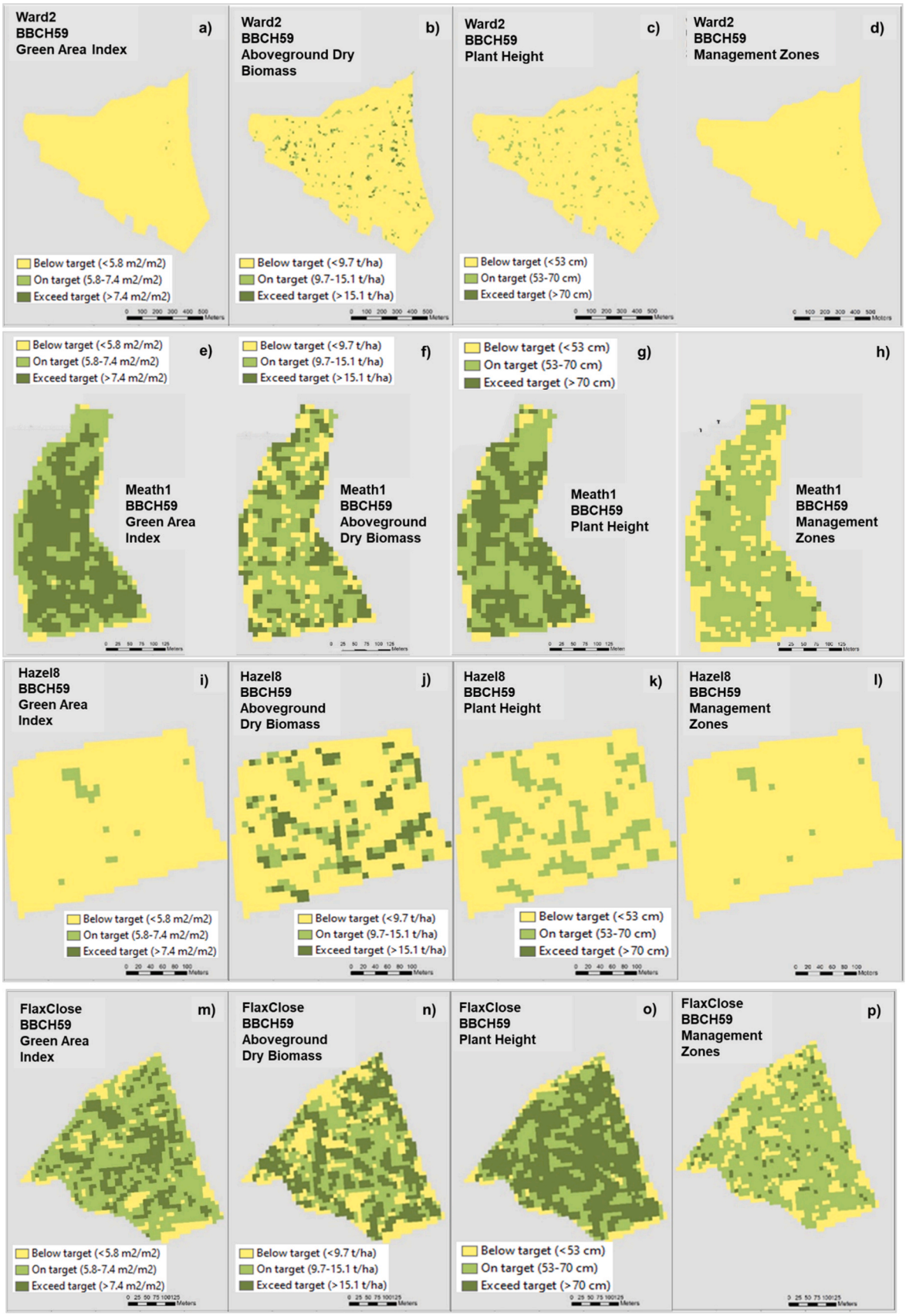

Fig. 12. Delineation of management zones in Ward2, Meath1, Hazel8, and FlaxClose wheat fields during BBCH 59 (Ear emerged) using GAI, AGDB and PH maps.

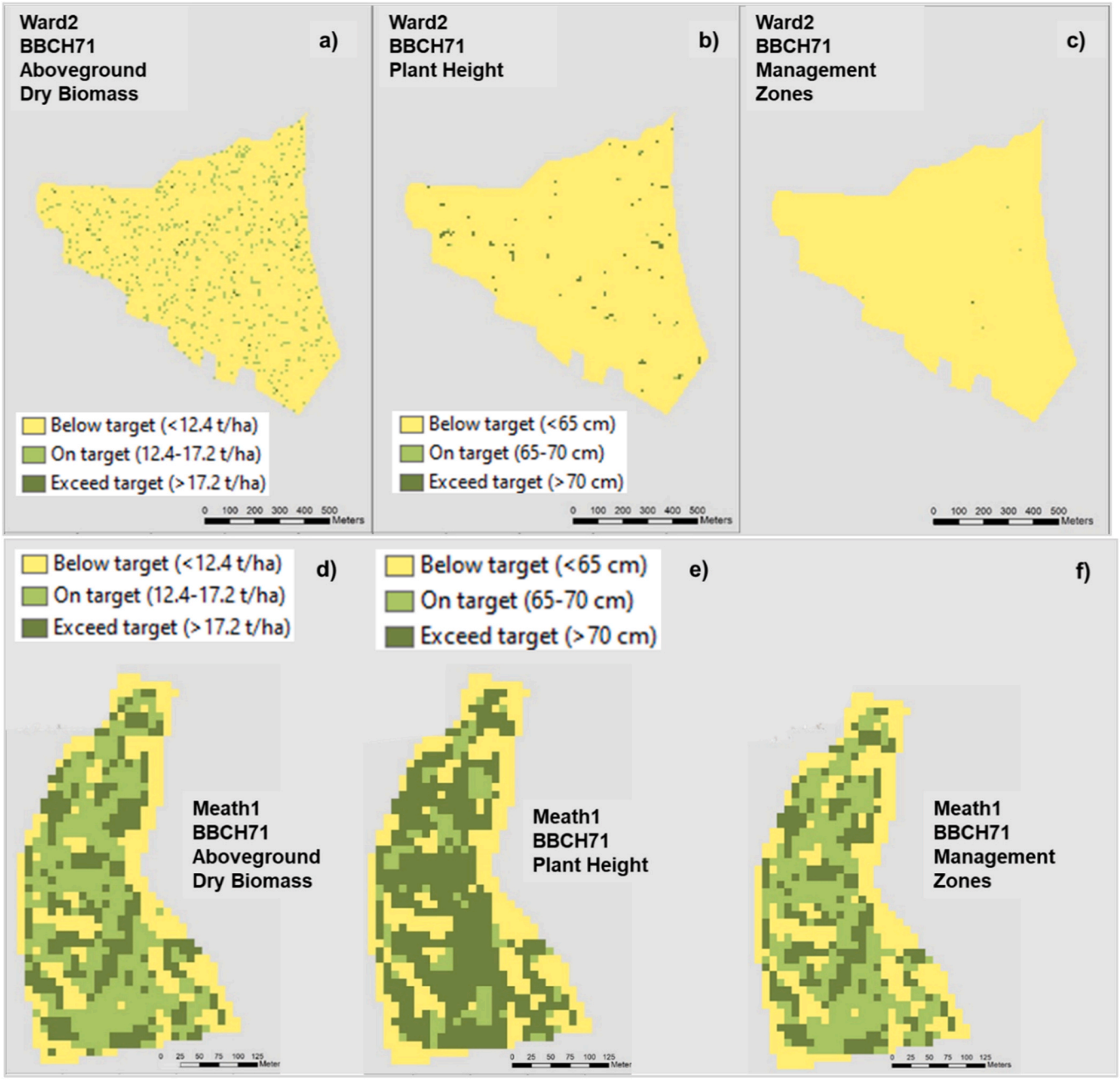

Fig. 13. Delineation of management zones in Ward2, Meath1, Hazel8 and FlaxClose wheat fields during BBCH 71 (Flowering completed) using AGDB and PH maps.

The management zone maps produced in this study provide a valuable representation of distinct patches within a field to serve as decision making tools for both farmers and agronomists. The management zone maps help to understand the variation of crop properties within field to address areas of low crop performance. Other than that, the management zone maps also serve as site-specific management practices, such as variable rate application of fertilizer, fungicide to optimize the profit and reduce chemical pollution to the environment. This information was further validated using site visit photos and feedback from the farmers. It is crucial to consider agronomic performance benchmark across different countries and crop types with similar plant traits to understand the potential yield and achieve balance between agriculture input and output when replicating this approach.

The research also implemented pixel level fusion by combining Sentinel-1 and Sentinel-2 data. Further assessment was done to find out the sensitivities of fusion data to different phenological stages. The study reveals that disparate performance over different growth stages and the models perform best during specific growth stage window when crop properties are actively developing. The backscatter and reflectance of remotely sensed data are determined by a series of morphological changes, structural characteristics difference [38].

The results showed that fusion sensor's model demonstrated stronger prediction power than single optical sensor. However, the radar backscatters influenced by the background soil variability and attenuating structures during BBCH 21–30 when NDVI < 0.7 [24,36]. Exceptional to the SD where single optical sensor showed highest prediction power. The variable importance also disclosed a single vegetation index lacked a distinct predictive correlation with specific biophysical properties.

The developed framework integrates winter wheat CBP with crop management, contributing to fundamental of Digital Twins in

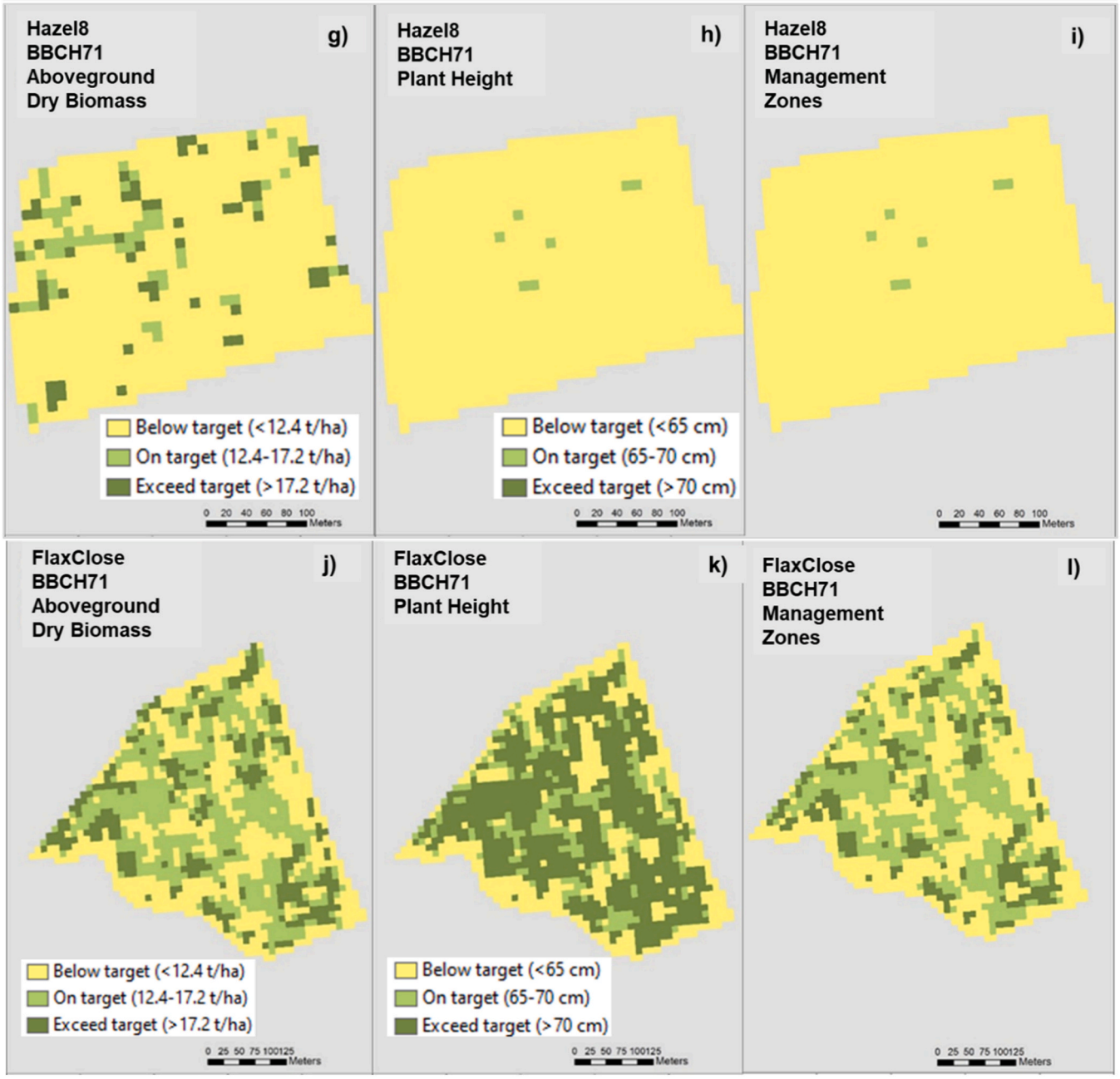

Fig. 13. (*continued*).

agriculture monitoring. Overall, this research bridges the gap between remote sensing technology, field management, and sustainable agricultural practices, fostering a more efficient and informed approach to crop production.

CRediT authorship contribution statement

Bing Bing Goh: Writing – original draft, Validation, Software, Methodology, Investigation, Formal analysis, Data curation, Conceptualization. **Nicholas M. Holden:** Writing – review & editing, Supervision, Investigation, Funding acquisition, Conceptualization. **Sheida Z Sattari:** Investigation, Writing – review & editing. **Chris J. Bleakley:** Writing – review & editing.

Declaration of Competing Interest

The authors declare that they have no known competing financial interests or personal relationships that could have appeared to influence the work reported in this paper.

Data availability

The data that has been used is confidential.

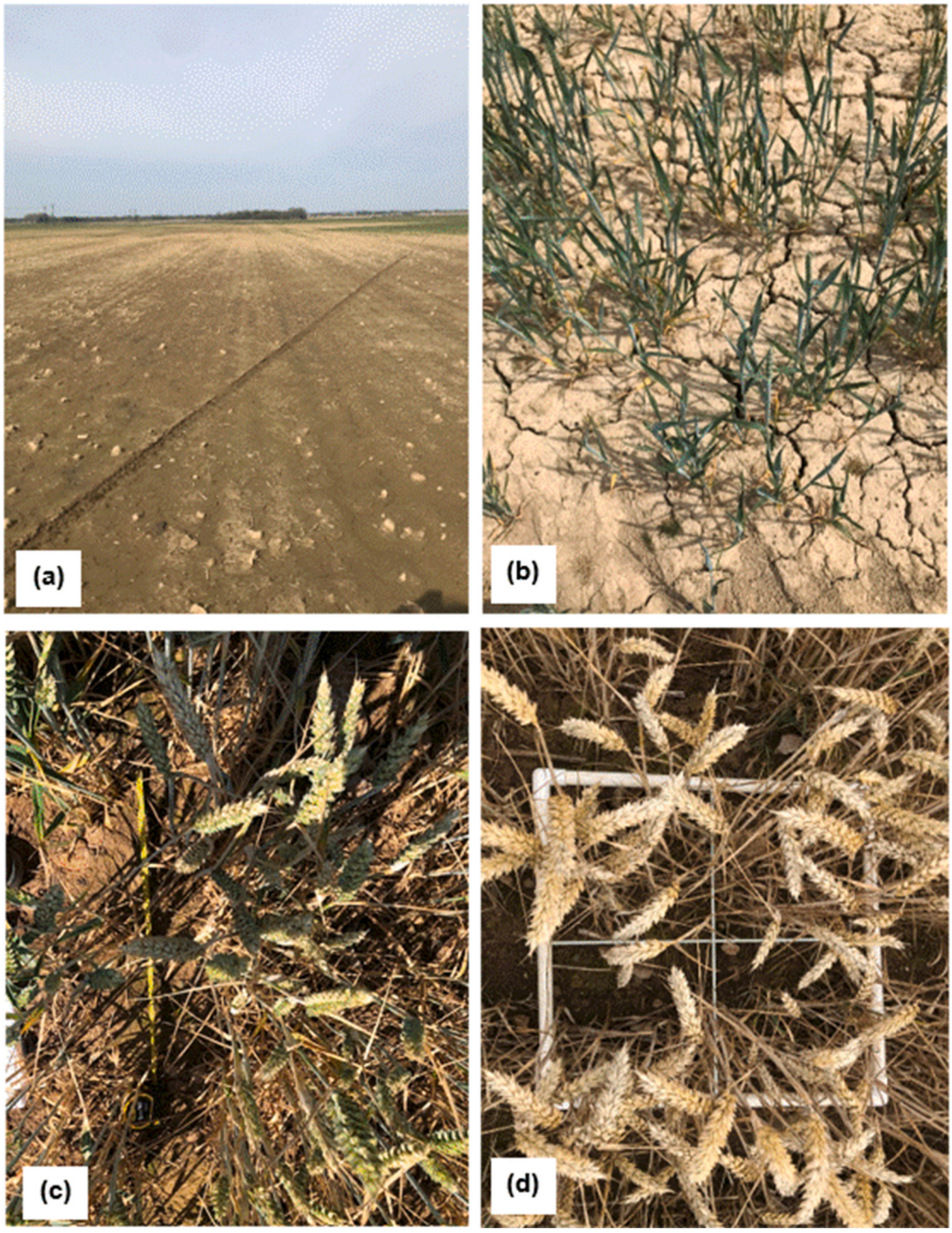

Fig. 14. Pictures of field visit (a) vast plain of bare soil with no winter wheat plant at Ward2 during tillering (b) Ward2 field covered with sparse tiny wheat plants during fruiting. (c) Hazel8 fields struck by drought during heading and flowering. (d) Early senescence of Hazel8 field during fruiting.

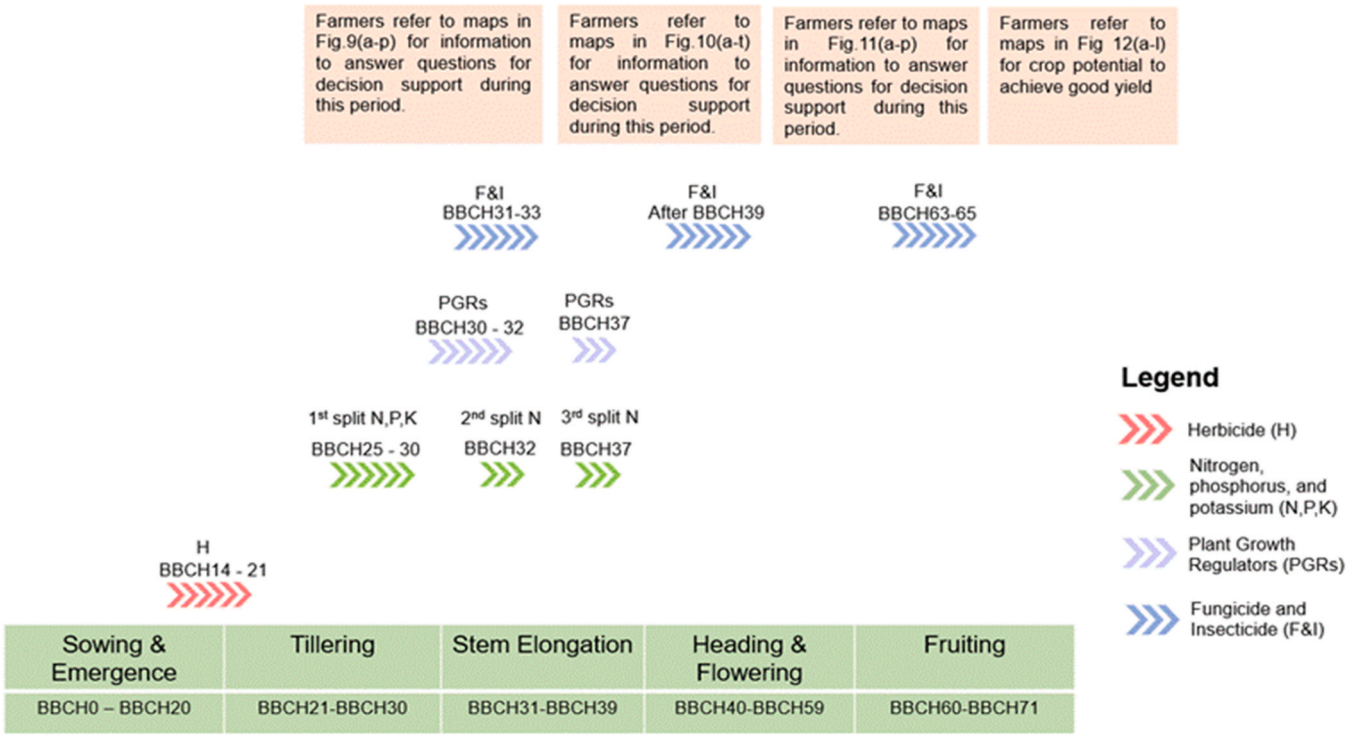

Fig. 15. Diagram of winter wheat crop management at 4 key growth stages and incorporate the crop biophysical property maps in as decision-making tool.

Acknowledgements

This research has been undertaken as part of the strategic partnership program between Science Foundation Ireland and ORIGIN Enterprises Limited, CONSUS funded under Grant Number 16/SPP/3296. We thank Andy Doyle, Robbie Byrne, and Lucy Cottingham for farmers' contact in IE and UK. We also thank postdoctoral staffs Dr Rebecca Whetton, Dr Gary Gillespie and Dr Jiwei Xu for their help with fieldwork.

Appendix A. Supporting information

Supplementary data associated with this article can be found in the online version at doi:10.1016/j.geomat.2024.100018.

References

[1] A. Nasrallah N. Baghdadi M. El Hajj T. Darwish H. Belhouchette G. Faour S. Darwich M. Mhawej Sentinel-1 data for winter wheat phenology monitoring and mapping Remote Sens. 11 2019 2228 doi: 10.3390/rs11192228.
[2] Alley, M., Thomason, W., Holshouser, D., Roberson, G.T., 2011. Precision Farming Tools: Variable-Rate Application. VCE, Variable Rate Application.
[3] B. Basso, D. Cammarano, C. Fiorentino, J.T. Ritchie, Wheat yield response to spatially variable nitrogen fertilizer in Mediterranean environment, Eur J. Agron. 51 (2013) 65–70, https://doi.org/10.1016/j.eja.2013.06.007.
[4] L.M. Bastos, W. Carciochi, R.P. Lollato, B.R. Jaenisch, C.R. Rezende, R. Schwalbert, P.V. Vara Prasad, G. Zhang, A.K. Fritz, C. Foster, Y. Wright, S. Young, P. Bradley, I. A. Ciampitti, Winter wheat yield response to plant density as a function of yield environment and tillering potential: a review and field studies, Front. Plant Sci. 11 (2020) 54, https://doi.org/10.3389/fpls.2020.00054.
[5] I.J. Bingham, D.R. Walters, M.J. Foulkes, N.D. Paveley, Crop traits and the tolerance of wheat and barley to foliar disease, Ann. Appl. Biol. 154 (2009) 159–173, https://doi.org/10.1111/j.1744-7348.2008.00291.x.
[6] F. Brubeck-Hernandez, T. Vladimirova, M. Pooley, R. Thompson, B. Knight, Zone management in precision agriculture using satellite imagery. 2019 NASA/ESA Conference on Adaptive Hardware and Systems (AHS). Presented at the 2019 NASA/ESA Conference on AHS, IEEE,, Colchester, United Kingdom, 2019, pp. 65–71, https://doi.org/10.1109/AHS.2019.00006.
[7] D. Chen, H. Suter, A. Islam, R. Edis, J.R. Freney, C.N. Walker, Prospects of improving efficiency of fertiliser nitrogen in Australian agriculture: a review of enhanced efficiency fertilisers, Soil Res. 46 (2008) 289, https://doi.org/10.1071/SR07197.
[8] M. Corti, P. Marino Gallina, D. Cavalli, B. Ortuani, G. Cabassi, G. Cola, A. Vigoni, L. Degano, S. Bregaglio, Evaluation of in-season management zones from high-resolution soil and plant sensors, Agronomy 10 (2020) 1124, https://doi.org/10.3390/agronomy10081124.
[9] D.L. Corwin, R.E. Plant, Applications of apparent soil electrical conductivity in precision agriculture, Comput. Electron Agric. 46 (2005) 1–10, https://doi.org/10.1016/j.compag.2004.10.004.
[10] D.R. Cutler, T.C. Edwards, K.H. Beard, A. Cutler, K.T. Hess, J. Gibson, J.J. Lawler, Random forests for classification in ecology, Ecology 88 (2007) 2783–2792, https://doi.org/10.1890/07-0539.1.
[11] M. Diacono, P. Rubino, F. Montemurro, Precision nitrogen management of wheat. A review, Agron. Sustain. Dev. 33 (2013) 219–241, https://doi.org/10.1007/s13593-012-0111-z.
[12] D. Ehlert, J. Schmerler, U. Voelker, Variable rate nitrogen fertilisation of winter wheat based on a crop density sensor, Precis. Agric. 5 (2004) 263–273, https://doi.org/10.1023/B:PRAG.0000032765.29172.ec.
[13] P. Ferrazzoli, S. Paloscia, P. Pampaloni, G. Schiavon, D. Solimini, P. Coppo, Sensitivity of microwave measurements to vegetation biomass and soil moisture content: a case study, IEEE Trans. Geosci. Remote Sens. 30 (1992) 750–756, https://doi.org/10.1109/36.158869.
[14] Z. Gao, Y. Wang, G. Tian, Y. Zhao, C. Li, Q. Cao, R. Han, Z. Shi, M. He, Plant height and its relationship with yield in wheat under different irrigation regime, Irrig. Sci. 38 (2020) 365–371, https://doi.org/10.1007/s00271-020-00678-z.
[15] A. Gavioli, E.G. de Souza, C.L. Bazzi, K. Schenatto, N.M. Betzek, Identification of management zones in precision agriculture: an evaluation of alternative cluster analysis methods, Biosyst. Eng. 181 (2019) 86–102, https://doi.org/10.1016/j.biosystemseng.2019.02.019.
[16] B.-B. Goh, P. King, R.L. Whetton, S.Z. Sattari, N.M. Holden, Monitoring winter wheat growth performance at sub-field scale using multitemporal Sentinel-2 imagery, Int J. Appl. Earth Obs. Geoinf. 115 (2022) 103124, https://doi.org/10.1016/j.jag.2022.103124.
[17] S. Griffin, J. Hollis, Plant growth regulators on winter wheat – yield benefits of variable rate application, Adv. Anim. Vet. Sci. 8 (2017) 233–237, https://doi.org/10.17582/S2040470017000267.
[18] G. Guven, H. Samkar, Examination of dimension reduction performances of PLSR and PCR techniques in data with multicollinearity, Iran. J. Sci. Technol. Trans. Sci. 43 (2019) 969–978, https://doi.org/10.1007/s40995-018-0565-1.
[19] E.R. Hunt, C.S.T. Daughtry, What good are unmanned aircraft systems for agricultural remote sensing and precision agriculture? Int. J. Remote Sens. 39 (2018) 5345–5376, https://doi.org/10.1080/01431161.2017.1410300.
[20] J. Hyles, M.T. Bloomfield, J.R. Hunt, R.M. Trethowan, B. Trevaskis, Phenology and related traits for wheat adaptation, Heredity 125 (2020) 417–430, https://doi.org/10.1038/s41437-020-0320-1.
[21] M.A. Islam, A.K. Obour, M.C. Saha, J.J. Nachtman, W.K. Cecil, R.E. Baumgartner, Grain yield, forage yield, and nutritive value of dual-purpose small grains in the central high plains of the USA, Crop. Manag. 12 (2013) 1–8, https://doi.org/10.1094/CM-2012-0154-RS.

[22] B.R. Jaenisch, L.B. Munaro, S.V.K. Jagadish, R.P. Lollato, Modulation of wheat yield components in response to management intensification to reduce yield gaps, Front. Plant Sci. 13 (2022) 772232, https://doi.org/10.3389/fpls.2022.772232.
[23] P. Janrao, H. Palivela, Management Zone Delineation in Precision Agriculture Using Data Mining: A Review. 2015 International Conference on Innovations in Information, Embedded and Communication Systems (ICIIECS). Presented at the 2015 International Conference on Innovations in Information,Embedded and Communication Systems (ICIIECS), IEEE,, Coimbatore, India, 2015, pp. 1–7, https://doi.org/10.1109/ICIIECS.2015.7193256.
[24] J.S. Jennewein, B.T. Lamb, W.D. Hively, A. Thieme, R. Thapa, A. Goldsmith, S. B. Mirsky, Integration of satellite-based optical and synthetic aperture radar imagery to estimate winter cover crop performance in cereal grasses, Remote Sens. 14 (2022) 2077, https://doi.org/10.3390/rs14092077.
[25] C.K. Johnson, J.W. Doran, H.R. Duke, B.J. Wienhold, K.M. Eskridge, J.F. Shanahan, Field-scale electrical conductivity mapping for delineating soil condition, Soil Sci. Soc. Am. J. 65 (2001) 1829–1837, https://doi.org/10.2136/sssaj2001.1829.
[26] M. Kazlauskas, E. Sarauskis, K. Romaneckas, D. Steponavicius, A. Jasinskas, V. Naujokiene, I. Bruciene, T. Ziogas, D. Vaicekauskas, J. Anusauskas, A. Mounem Mouazen, Effect of variable rate seeding on winter wheat seedbed and germination parameters using soil apparent electrical conductivity, Presente 20th Int. Sci. Conf. Eng. Rural Dev. (2021) https://doi.org/10.22616/ERDev.2021.20.TF240.
[27] B. Koch, R. Khosla, W.M. Frasier, D.G. Westfall, D. Inman, Economic feasibility of variable-rate nitrogen application utilizing site-specific management zones, Agron. J. 96 (2004) 1572–1580, https://doi.org/10.2134/agronj2004.1572.
[28] Konica Minolta, 2009. Chlorophyll Meter Spad-502plus, [WWW Document], Konica Minolta, URL https://www.konicaminolta.com/instruments/download/catalog/color/pdf/spad502plus_catalog_eng.pdf (accessed 5.30.22).
[29] D. Li, X. Wang, H. Zheng, K. Zhou, X. Yao, Y. Tian, Y. Zhu, W. Cao, T. Cheng, Estimation of area- and mass-based leaf nitrogen contents of wheat and rice crops from water-removed spectra using continuous wavelet analysis, Plant Methods 14 (1) (2018) 76, https://doi.org/10.1186/s13007-018-0344-1 [online].
[30] X. Li, W. Zhao, J. Li, Y. Li, Maximizing water productivity of winter wheat by managing zones of variable rate irrigation at different deficit levels, Agric. Water Manag. 216 (2019) 153–163, https://doi.org/10.1016/j.agwat.2019.02.002.
[31] J.P. Lynch, D. Doyle, S. McAuley, F. McHardy, Q. Danneels, L.C. Black, E.M. White, J. Spink, The impact of variation in grain number and individual grain weight on winter wheat yield in the high yield potential environment of Ireland, Eur J. Agron. 87 (2017) 40–49, https://doi.org/10.1016/j.eja.2017.05.001.
[32] C. Ma, P. Xie, K. Zhang, J. Yang, X. Li, F. Liu, L. Lin, H. Zhang, Contribution of the flag leaf to lead absorption in wheat grain at the grain-filling stage, Ecotoxicol. Environ. Saf. 225 (2021) 112722, https://doi.org/10.1016/j.ecoenv.2021.112722.
[33] G. Macelloni, S. Paloscia, P. Pampaloni, F. Marliani, M. Gai, The relationship between the backscattering coefficient and the biomass of narrow and broad leaf crops, IEEE Trans. Geosci. Remote Sens. 39 (2001) 873–884, https://doi.org/10.1109/36.917914.
[34] H. Mäkinen, J. Kaseva, M. Trnka, J. Balek, K.C. Kersebaum, C. Nendel, A. Gobin, J. E. Olesen, M. Bindi, R. Ferrise, M. Moriondo, A. Rodríguez, M. Ruiz-Ramos, J. Takáč, P. Bezák, D. Ventrella, F. Ruget, G. Capellades, H. Kahiluoto, Sensitivity of European wheat to extreme weather, Field Crops Res. 222 (2018) 209–217, https://doi.org/10.1016/j.fcr.2017.11.008.
[35] D. Mandal, V. Kumar, H. McNairn, A. Bhattacharya, Y.S. Rao, Joint estimation of Plant Area Index (PAI) and wet biomass in wheat and soybean from C-band polarimetric SAR data, Int. J. Appl. Earth Obs. Geoinf. 79 (2019) 24–34, https://doi.org/10.1016/j.jag.2019.02.007.
[36] F. Mattia, Thuy Le Toan, G. Picard, F.I. Posa, A. D'Alessio, C. Notarnicola, A. M. Gatti, M. Rinaldi, G. Satalino, G. Pasquariello, Multitemporal c-band radar measurements on wheat fields, IEEE Trans. Geosci. Remote Sens. 41 (2003) 1551–1560, https://doi.org/10.1109/TGRS.2003.813531.
[37] A. Nezhadahmadi, Z.H. Prodhan, G. Faruq, Drought tolerance in wheat, Sci. World J. 2013 (2013) 1–12, https://doi.org/10.1155/2013/610721.
[38] S.V. Ollinger, Sources of variability in canopy reflectance and the convergent properties of plants, N. Phytol. 189 (2011) 375–394, https://doi.org/10.1111/j.1469-8137.2010.03536.x.
[39] Paloscia , S. , Macelloni , G. , Pampaloni , P. , 1998. The Relations between Backscattering Coefficient and Biomass of Narrow and Wide Leaf Crops, in: IGARSS '98. Sensing and Managing the Environment. 1998 IEEE International Geoscience and Remote Sensing. Symposium Proceedings. (Cat. No.98CH36174). Presented at the IGARSS '98. Sensing and Managing the Environment. 1998 IEEE International Geoscience and Remote Sensing. Symposium Proceedings. (Cat. No.98CH36174), IEEE, Seattle, WA, USA, pp. 100–102 vol.1. https://doi.org/10.1109/IGARSS.1998.702811.
[40] A.S. Peake, K.L. Bell, R.A. Fischer, M. Gardner, B.T. Das, N. Poole, M. Mumford, Cultivar × management interaction to reduce lodging and improve grain yield of irrigated spring wheat: optimising plant growth regulator use, N application timing, row spacing and sowing date, Front. Plant Sci. 11 (2020) 401, https://doi.org/10.3389/fpls.2020.00401.
[41] M. Peña-Gallardo, S.M. Vicente-Serrano, S. Quiring, M. Svoboda, J. Hannaford, M. Tomas-Burguera, N. Martín-Hernández, F. Domínguez-Castro, A. El Kenawy, Response of crop yield to different time-scales of drought in the United States: Spatio-temporal patterns and climatic and environmental drivers, Agric. Meteor. 264 (2019) 40–55, https://doi.org/10.1016/j.agrformet.2018.09.019.
[42] M. Pérez-Ruiz, P. Gonzalez-de-Santos, A. Ribeiro, C. Fernandez-Quintanilla, A. Peruzzi, M. Vieri, S. Tomic, J. Agüera, Highlights and preliminary results for autonomous crop protection, Comput. Electron Agric. 110 (2015) 150–161, https://doi.org/10.1016/j.compag.2014.11.010.
[43] R. Qin, C. Noulas, D. Wysocki, X. Liang, G. Wang, S. Lukas, Application of plant growth regulators on soft white winter wheat under different nitrogen fertilizer scenarios in irrigated fields, Agriculture 10 (2020) 305, https://doi.org/10.3390/agriculture10070305.
[44] Y. Ren, W. Huang, H. Ye, X. Zhou, H. Ma, Y. Dong, Y. Shi, Y. Geng, Y. Huang, Q. Jiao, Q. Xie, Quantitative identification of yellow rust in winter wheat with a new spectral index: development and validation using simulated and experimental data, Int J. Appl. Earth Obs. Geoinf. 102 (2021) 102384, https://doi.org/10.1016/j.jag.2021.102384.
[45] L. Sharma, S. Bali, A review of methods to improve nitrogen use efficiency in agriculture, Sustainability 10 (2017) 51, https://doi.org/10.3390/su10010051.
[46] K. Sieling, U. Böttcher, H. Kage, Growth stage specific optima for the green area index of winter wheat, Field Crops Res 148 (2013) 34–42, https://doi.org/10.1016/j.fcr.2013.04.002.
[47] R.P. Sishodia, R.L. Ray, S.K. Singh, Applications of remote sensing in precision agriculture: a review, Remote Sens 12 (2020) 3136, https://doi.org/10.3390/rs12193136.
[48] T. Sivasankar, D. Kumar, H.S. Srivastava, P. Patel, Advances in Radar Remote Sensing of Agricultural Crops: A Review, Int. J. Adv. Sci. Eng. Inf. Techno 8 (4) (2018) 1126, https://doi.org/10.18517/ijaseit.8.4.5797 [online].
[49] X. Song, J. Wang, W. Huang, L. Liu, G. Yan, R. Pu, The delineation of agricultural management zones with high resolution remotely sensed data, Precis. Agric. 10 (2009) 471–487, https://doi.org/10.1007/s11119-009-9108-2.
[50] D. Spaner, A.G. Todd, A. Navabi, D.B. McKenzie, L.A. Goonewardene, Can leaf chlorophyll measures at differing growth stages be used as an indicator of winter wheat and spring barley nitrogen requirements in Eastern Canada? J. Agron. Crop Sci. 191 (2005) 393–399, https://doi.org/10.1111/j.1439-037X.2005.00175.x.
[51] A. Srinivasan, Handbook of Precision Agriculture: Principles and Applications, Food Products Press,, Bringhamton, NY, 2006.
[52] Sylvester-Bradley, R., Berry, P., Blake, J., Kindred, D., Spink, J., Bingham, I., McVittie, J., Foulkes, J., 2018. Wheat Growth Guide. AHDB Cereals & Oilseeds.
[53] M.S. Tilley, R.W. Heiniger, C.R. Crozier, Tiller initiation and its effects on yield and yield components in winter wheat, Agron. J. 111 (2019) 1323–1332, https://doi.org/10.2134/agronj2018.07.0469.
[54] C. Verdouw, B. Tekinerdogan, A. Beulens, S. Wolfert, Digital twins in smart farming, Agric. Syst. 189 (2021) 103046, https://doi.org/10.1016/j.agsy.2020.103046.
[55] I. Vilmus, M. Ecarnot, N. Verzelen, P. Roumet, Monitoring nitrogen leaf resorption kinetics by near-infrared spectroscopy during grain filling in durum wheat in different nitrogen availability conditions, Crop Sci. 54 (2014) 284–296, https://doi.org/10.2135/cropsci2013.02.0099.
[56] E. Vrindts, A.M. Mouazen, M. Reyniers, K. Maertens, M.R. Maleki, H. Ramon, J. De Baerdemaeker, Management zones based on correlation between soil compaction, yield and crop data, Biosyst. Eng. 92 (2005) 419–428, https://doi.org/10.1016/j.biosystemseng.2005.08.010.
[57] L. Wang, J. Sun, C. Wang, Z. Shangguan, Leaf photosynthetic function duration during yield formation of large-spike wheat in rainfed cropping systems, PeerJ 6 (2018) e5532, https://doi.org/10.7717/peerj.5532.
[58] Y. Wang, J. Zhao, W. Lu, D. Deng, Gibberellin in plant height control: old player, new story, Plant Cell Rep. 36 (2017) 391–398, https://doi.org/10.1007/s00299-017-2104-5.
[59] L. Wang, X. Zhou, X. Zhu, Z. Dong, W. Guo, Estimation of biomass in wheat using random forest regression algorithm and remote sensing data, Crop J. 4 (2016) 212–219, https://doi.org/10.1016/j.cj.2016.01.008.
[60] W. Zhao, J. Li, R. Yang, Y. Li, Crop yield and water productivity responses in management zones for variable-rate irrigation based on available soil water holding capacity, Trans. ASABE 60 (2017) 1659–1667, https://doi.org/10.13031/trans.12340.